Article

Cell Host & Microbe

Cyclopropane Modification of Trehalose Dimycolate Drives Granuloma Angiogenesis and Mycobacterial Growth through Vegf Signaling

Graphical Abstract

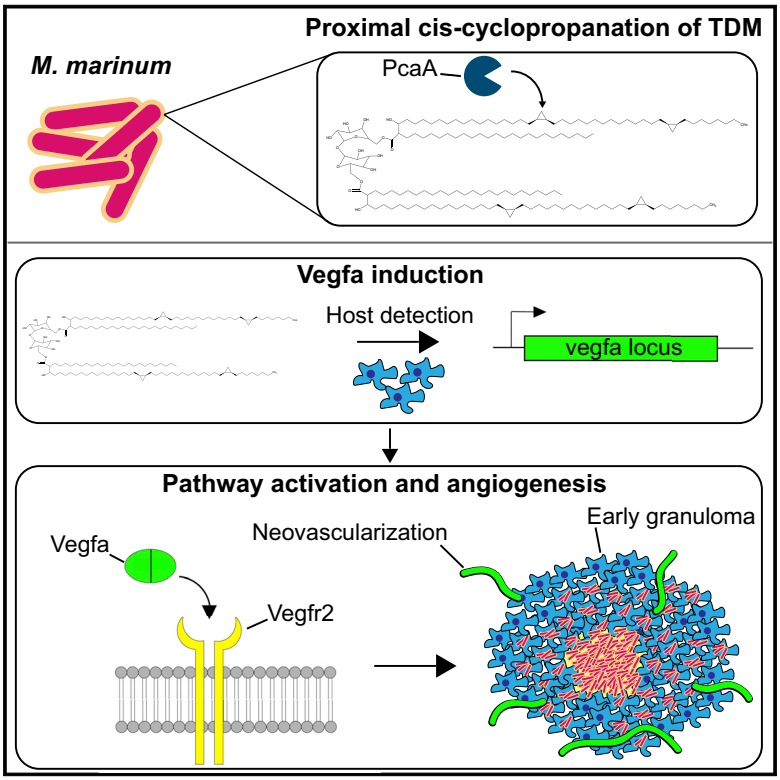

Highlights

- Mycobacterial granuloma angiogenesis requires the cell wall glycolipid TDM
- The mycobacterial enzyme PcaA promotes angiogenesis via *cis*-cyclopropanation of TDM
- Cyclopropanated TDM induces granuloma vascularization through activating Vegfa signaling
- *pcaA* mutation or Vegfa pathway blockade reduces bacterial growth *in vivo*

Authors

Eric M. Walton, Mark R. Cronan, C.J. Cambier, ..., Didier Y.R. Stainier, Carolyn R. Bertozzi, David M. Tobin

Correspondence

david.tobin@duke.edu

In Brief

Granuloma formation during tuberculosis is accompanied by remodeling of host vasculature. Walton et al. identify the mycobacterial enzyme PcaA, which catalyzes proximal *cis*-cyclopropanation of trehalose dimycolate, as an important determinant of granuloma-associated angiogenesis. This form of trehalose dimycolate induces Vegfa-mediated angiogenesis at the granuloma, promoting bacterial growth.

Walton et al., 2018, Cell Host & Microbe *24*, 514–525
October 10, 2018
https://doi.org/10.1016/j.chom.2018.09.004

CellPress

CellPress

Cell Host & Microbe
Article

Cyclopropane Modification of Trehalose Dimycolate Drives Granuloma Angiogenesis and Mycobacterial Growth through Vegf Signaling

Eric M. Walton,[1] Mark R. Cronan,[1] C.J. Cambier,[2] Andrea Rossi,[3] Michele Marass,[3] Matthew D. Foglia,[4,5] W. Jared Brewer,[1] Kenneth D. Poss,[4,5] Didier Y.R. Stainier,[3] Carolyn R. Bertozzi,[2,6] and David M. Tobin[1,7,8,*]
[1]Department of Molecular Genetics and Microbiology, Duke University School of Medicine, Durham, NC 27710, USA
[2]Department of Chemistry, Stanford University, Stanford, CA 94305, USA
[3]Department of Developmental Genetics, Max Planck Institute for Heart and Lung Research, Bad Nauheim, Germany
[4]Department of Cell Biology, Duke University School of Medicine, Durham, NC 27710, USA
[5]Regeneration Next, Duke University, Durham, NC 27710, USA
[6]Howard Hughes Medical Institute, Stanford University, Stanford, CA 94305, USA
[7]Department of Immunology, Duke University School of Medicine, Durham, NC 27710, USA
[8]Lead Contact
*Correspondence: david.tobin@duke.edu
https://doi.org/10.1016/j.chom.2018.09.004

SUMMARY

Mycobacterial infection leads to the formation of characteristic immune aggregates called granulomas, a process accompanied by dramatic remodeling of the host vasculature. As granuloma angiogenesis favors the infecting mycobacteria, it may be actively promoted by bacterial determinants during infection. Using *Mycobacterium marinum*-infected zebrafish as a model, we identify the enzyme proximal cyclopropane synthase of alpha-mycolates (PcaA) as an important bacterial determinant of granuloma-associated angiogenesis. *cis*-Cyclopropanation of mycobacterial mycolic acids by *pcaA* drives the activation of host Vegf signaling within granuloma macrophages. Cyclopropanation of the mycobacterial cell wall glycolipid trehalose dimycolate is both required and sufficient to induce robust host angiogenesis. Inducible genetic inhibition of angiogenesis and Vegf signaling during granuloma formation results in bacterial growth deficits. Together, these data reveal a mechanism by which PcaA-mediated *cis*-cyclopropanation of mycolic acids promotes bacterial growth and dissemination *in vivo* by eliciting granuloma vascularization and suggest potential approaches for host-directed therapies.

INTRODUCTION

Upon entry into the lung, *Mycobacterium tuberculosis* is initially phagocytosed by host macrophages. Pathogenic mycobacteria evade the initial antimicrobial response through a variety of mechanisms, and infected and uninfected macrophages form characteristic aggregates that mature into tightly organized structures called granulomas (Ernst, 2012; Pagan and Ramakrishnan, 2018). The resulting environment provides a spatially restricted focus of infection that infecting mycobacteria have adapted to and can exploit (Pagan and Ramakrishnan, 2018; Rittershaus et al., 2013).

In addition to immune cell populations, stromal cells proximal to the granuloma undergo substantial reprogramming and remodeling. Analysis of human clinical specimens and a number of animal models revealed induction of Vegf family members by granuloma macrophages and extensive granuloma vascularization (Datta et al., 2015; Harding et al., 2015; Kumar et al., 2016; Oehlers et al., 2015; Polena et al., 2016). In tumor biology there is extensive interplay between angiogenesis and hypoxia, and, similarly, mycobacterial granulomas in both animal models and humans can develop hypoxic regions (Aly et al., 2007; Folkman, 2002; Oehlers et al., 2015; Tsai et al., 2006; Ulrichs et al., 2005). Notably, mycobacterially induced angiogenesis at the granuloma promotes bacterial growth *in vivo*; nascent blood vessels associated with early granulomas may provide oxygen and nutrients, and can create a permissive replication niche for the bacteria within (Datta et al., 2015; Oehlers et al., 2015, 2017). Pharmacological limitation of granuloma-associated angiogenesis or vascular normalization results in improved host outcomes in animal models of infections (Oehlers et al., 2015, 2017; Polena et al., 2016). As granuloma angiogenesis favors the infecting mycobacteria, it is likely that this host response may be actively promoted, enhanced, or accelerated by bacterial determinants during infection.

Mycolic acids are present in the cell walls of certain *Actinomycetes*, and have been associated with virulence for human and animal pathogens from genera such as *Mycobacterium* and *Rhodococcus* (Barry et al., 1998; Sydor et al., 2013). Of the mycolic acid-containing lipids, trehalose-6,6-dimycolate (TDM) is particularly abundant within the outer cell wall of *M. tuberculosis* (Brennan and Nikaido, 1995). TDM has been described as a potent adjuvant and is associated with a number of aspects of mycobacterial disease pathogenesis, including limitation of phagolysosome fusion and activation of matrix metalloproteases (Axelrod et al., 2008; Hunter et al., 2006; Indrigo et al., 2003; Middlebrook et al., 1947; Patin et al., 2017; Sakamoto et al., 2013).

Studies of host recognition of TDM have implicated diverse cell surface proteins, including Toll-like receptors, lectins, and scavenger receptors (Bowdish et al., 2009; Lang, 2013; Miyake et al., 2015; Richardson and Williams, 2014). Thus, TDM may act through multiple signaling pathways as a major modulator of the host immune response to mycobacteria. To date, however, relatively little attention has been paid to the angiogenic potential of TDM, although TDM can induce angiogenesis in a rat corneal model (Saita et al., 2000).

TDM is essential for mycobacterial viability *in vivo*, but a number of chemical modifications that occur within the mycolic acid tails of TDM can be genetically targeted. The three major classes of mycolic acids (alpha, keto, and methoxy) incorporate double bonds or cyclopropyl groups into the proximal position of the meromycolate chain and double bonds, cyclopropyl groups, ketones, or methoxy groups into the distal position (Brennan and Besra, 1997). These non-essential chemical modifications can be genetically altered to study *in vivo* infection phenotypes (Glickman et al., 2000, 2001).

Notably, functionalization at the proximal position with a cyclopropyl group is associated with pathogenic species of mycobacteria; the mycolates from *M. tuberculosis*, *M. avium*, *M. ulcerans*, and *M. marinum* contain cylcopropyl groups at this position, while non-pathogenic species such as *M. smegmatis* and *M. chelonae* possess a double bond (Daffe et al., 1991; Liu et al., 1996). In addition, an enzyme that catalyzes the addition of *cis*-cyclopropyl groups to the proximal end of mycolic acids of the alpha-mycolate class, PcaA, has been implicated in virulence (Glickman et al., 2000). In murine models, *pcaA* mutants display an *in vivo* growth defect at 1 week post-infection, concomitant with a reduced pro-inflammatory cytokine response from macrophages (Glickman et al., 2000; Rao et al., 2005). However, the influence of mycolic acid modifications on granuloma-associated angiogenesis has not been examined.

We have previously utilized the zebrafish/*M. marinum* model of infection to study angiogenesis during mycobacterial infection and granuloma formation (Oehlers et al., 2015). The zebrafish is a natural host to *M. marinum*, a close relative of the *M. tuberculosis* complex (Tobin and Ramakrishnan, 2008). Mycobacterial pathogenesis in zebrafish closely resembles that of human tuberculosis, from macrophage aggregation and vascularization to the formation of necrotic and hypoxic granulomas (Cronan et al., 2016; Davis et al., 2002; Oehlers et al., 2015; Swaim et al., 2006). Using *M. marinum* mutant strains, we demonstrate that PcaA-mediated modifications to TDM are required to elicit a robust angiogenic response during mycobacterial infection. We describe *in vivo* growth defects for *pcaA* mutants that coincide with the onset of granuloma vascularization. Furthermore, we demonstrate that the growth advantage of wild-type bacteria over *pcaA* mutants is Vegf dependent. Together, these data identify a role for TDM in angiogenesis-driven mycobacterial expansion via Vegf induction and identify the proximal *cis*-cyclopropyl modification of mycolic acid tails as crucial for TDM-mediated angiogenesis.

RESULTS

PcaA Deficiency Leads to Defects in Host Angiogenesis

To visualize vasculature within larval zebrafish, we used the *Tg(kdrl:EGFP)*^{s843} transgenic line in which EGFP expression is driven by the zebrafish *kdrl* promoter and labels all vasculature (Jin et al., 2005). Vasculature in the larval trunk forms a stereotypical pattern around the somites (Figure 1A). After dorsal infection with *M. marinum*, analysis of granulomas in the trunk provides a ready and quantifiable measure of angiogenesis in live animals (Figure 1B).

As we had previously found that host angiogenesis benefits infecting mycobacteria, we hypothesized that specific bacterial factors directly promote angiogenesis. The lipid-rich mycobacterial cell wall is a key interface between pathogen and host, and a number of lipid species have been identified that modify the host immune response (Brennan, 2003). The most abundant of these is TDM, a lipid known to interact with diverse host immune pathways. Deletion of the *M. tuberculosis pcaA* gene results in bacteria with an atypical pool of cell wall mycolic acids. *pcaA* mutants lack proximal *cis*-cyclopropyl alpha-mycolates and exhibit reduced proportions overall of both free alpha-mycolates and TDM of the alpha-mycolate class (Glickman et al., 2000; Rao et al., 2005). Despite these alterations to the cell envelope, Δ*pcaA M. tuberculosis* remain viable during infection. We hypothesized that disruption of *M. marinum pcaA* gene would confer similar cell wall alterations without compromising pathogen viability, providing an opportunity to probe the importance of TDM in granuloma-associated angiogenesis.

Using a defined *M. marinum* transposon library, we isolated two transposon mutants in the *M. marinum pcaA* gene (C. Cosma and L. Ramakrishnan). The mutants, designated *pcaA*^{Tn28776} and *pcaA*^{Tn20324}, possessed independent transposon insertions, in opposite orientations, ~10% of the way through the open reading frame. There were no significant differences in *in vitro* growth rates between wild-type *M. marinum* and the transposon mutants, with doubling times for wild-type, *pcaA*^{Tn28776}, and *pcaA*^{Tn20324} of 11.3, 11.7, and 10.9 hr, respectively, under the conditions assayed.

We constructed fluorescent versions of each transposon strain to image both infection and angiogenesis *in vivo*. Both *pcaA* mutants exhibited severe defects in granuloma-associated vascularization (Figure 1B). Decreased angiogenesis in the *pcaA* mutants was observed from the outset of vascularization in paired wild-type infections, at approximately 4 days post-infection (dpi) (Figures 1B and 1C) and persisted at later time points (Figures 1E and 1F). This phenotype could be rescued through expression of PcaA using a constitutive promoter (Figures 1B, 1D, and 1E). Granulomas formed normally in the *pcaA* mutants. Differences in granuloma-associated angiogenesis could be observed at 3 dpi, the earliest time point at which vascularization could be observed in wild-type infections, suggesting a potentially early and direct interaction of TDM with the host.

TDM Is Sufficient to Induce Angiogenesis

Based on the strong genetic requirement for *pcaA* for robust granuloma vascularization, we asked whether TDM might directly induce angiogenesis. To perform TDM sufficiency experiments, we developed a method to administer highly hydrophobic TDM into the zebrafish trunk. We found that we could inject mineral oil and surfactant (incomplete Freund's adjuvant) at 2 days post-fertilization (dpf) to generate stable, persistent droplets within the larvae. We then injected vehicle control or purified

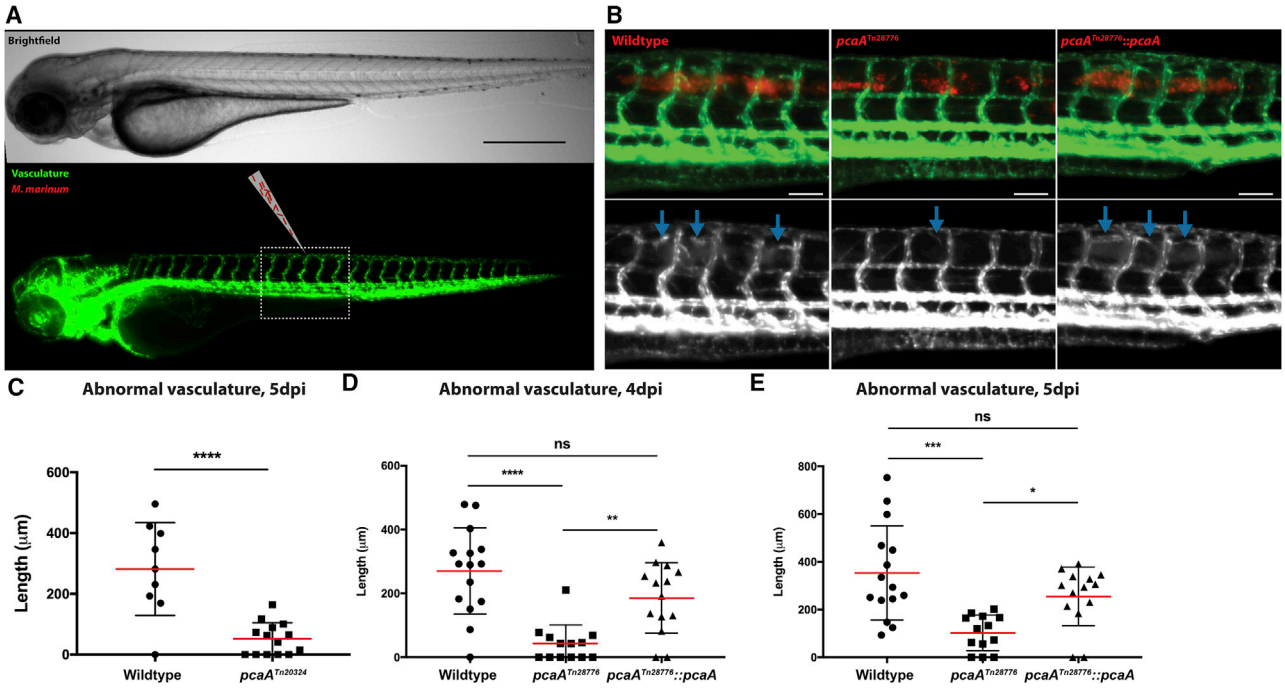

Figure 1. Mutations in *pcaA* Result in Angiogenesis-Deficient Infection Foci

(A) Depiction of the *M. marinum* injection site within the trunk of a zebrafish larva. Bright-field and GFP channels (upper and lower panels, respectively) are shown for clarity. Dotted line indicates approximate area shown for images in (B). Scale bar, 500 μm.

(B–E) Representative images of larvae at 4 days post-infection (dpi) infected with either wild-type, $pcaA^{Tn28776}$, or complemented mutant *M. marinum*. Bacteria in red, vasculature in green (upper panels) or white (lower panels). Blue arrows denote infection-associated angiogenesis (B). Length of abnormal vasculature at 5 dpi for infections with $pcaA^{Tn20324}$ (C) and 4 and 5 dpi for $pcaA^{Tn28776}$ (D and E). Representative of more than three independent experiments for each mutant. Scale bars, 100 μm. For experiment involving $pcaA^{Tn20324}$, ****$p < 0.0001$; Student's t test. For all other statistics, *$p < 0.05$; **$p < 0.01$; ***$p < 0.001$; ****$p < 0.0001$; one-way ANOVA with Tukey's multiple comparison post-test.

alpha-mycolate TDM from *M. bovis* dissolved in vehicle into the trunks of *Tg(kdrl:EGFP)* larvae at 2 dpf (Figure 2A). By 2 dpi, there was little or no abnormal vasculature in the vehicle-injected animals (Figures 2B and 2C). In contrast, TDM-containing droplets induced substantial abnormal vasculature, which associated spatially with the TDM-loaded droplets (Figures 2B and 2C). These results suggested that TDM is sufficient to evoke robust angiogenesis and, combined with the genetic mutant data, suggested a direct role for TDM in granuloma-associated angiogenesis.

Given the sufficiency of alpha-mycolate TDM in inducing angiogenesis and the requirement of mycobacterial *pcaA* for *in vivo* infection-induced angiogenesis, we hypothesized that PcaA-modified mycolates must be incorporated into TDM to be pro-angiogenic *in vivo*. However, it has been shown previously that free mycolic acid methyl esters (MAMEs) are also modified by PcaA, leaving open the possibility that these too contribute to PcaA-dependent angiogenesis (Glickman et al., 2000). Thin-layer chromatography (TLC) analysis of the TDM used in the previous experiments contained only alpha-mycolates (Figure S1A). Since oxygenated mycolates (methoxy- and keto-mycolates) have been previously identified as important for the virulence of *M. tuberculosis* (Dubnau et al., 2000), we wondered if these species would enhance or otherwise alter the angiogenic potential we observed for pure alpha-mycolate TDM.

To test these hypotheses, we compared the angiogenic effects of bulk TDM and bulk MAMEs isolated from *M. tuberculosis*, both of which possess mycolic acids modified by PcaA as well as the primary oxygenated mycolate species. We injected *Tg(kdrl:EGFP)* larvae with either TDM (2 mg/mL) or MAMEs (2 mg/mL) at 2 dpf and assessed abnormal vascularization at 4 dpf. TDM from *M. tuberculosis* induced robust angiogenesis (Figures S2A and S2B), achieving levels of vascularization comparable with TDM from *M. bovis*. The MAMEs, however, did not induce angiogenesis above vehicle alone (Figures S2C and S2D). Together, these data support the role of PcaA-modified TDM specifically, and not merely mycolic acids in general, as the critical inducer of PcaA-dependent angiogenesis. The sufficiency of pure alpha-mycolate TDM in inducing angiogenesis along with a lack of enhancement of this phenotype when oxygenated mycolates are present strongly supports alpha-mycolate TDM as the isoform responsible for driving vascularization.

The requirement that the *cis*-cyclopropyl alpha-mycolates be incorporated into TDM in order to elicit angiogenesis suggested that host receptors for TDM might be involved in initiating this process. To begin to probe this mechanism, we focused on Myd88- and FcRγ-dependent signaling pathways, both of which have been implicated in host responses to TDM (Bowdish et al., 2009; Geisel et al., 2005; Lobato-Pascual et al., 2013; Miyake et al., 2013; Werninghaus et al., 2009). We generated

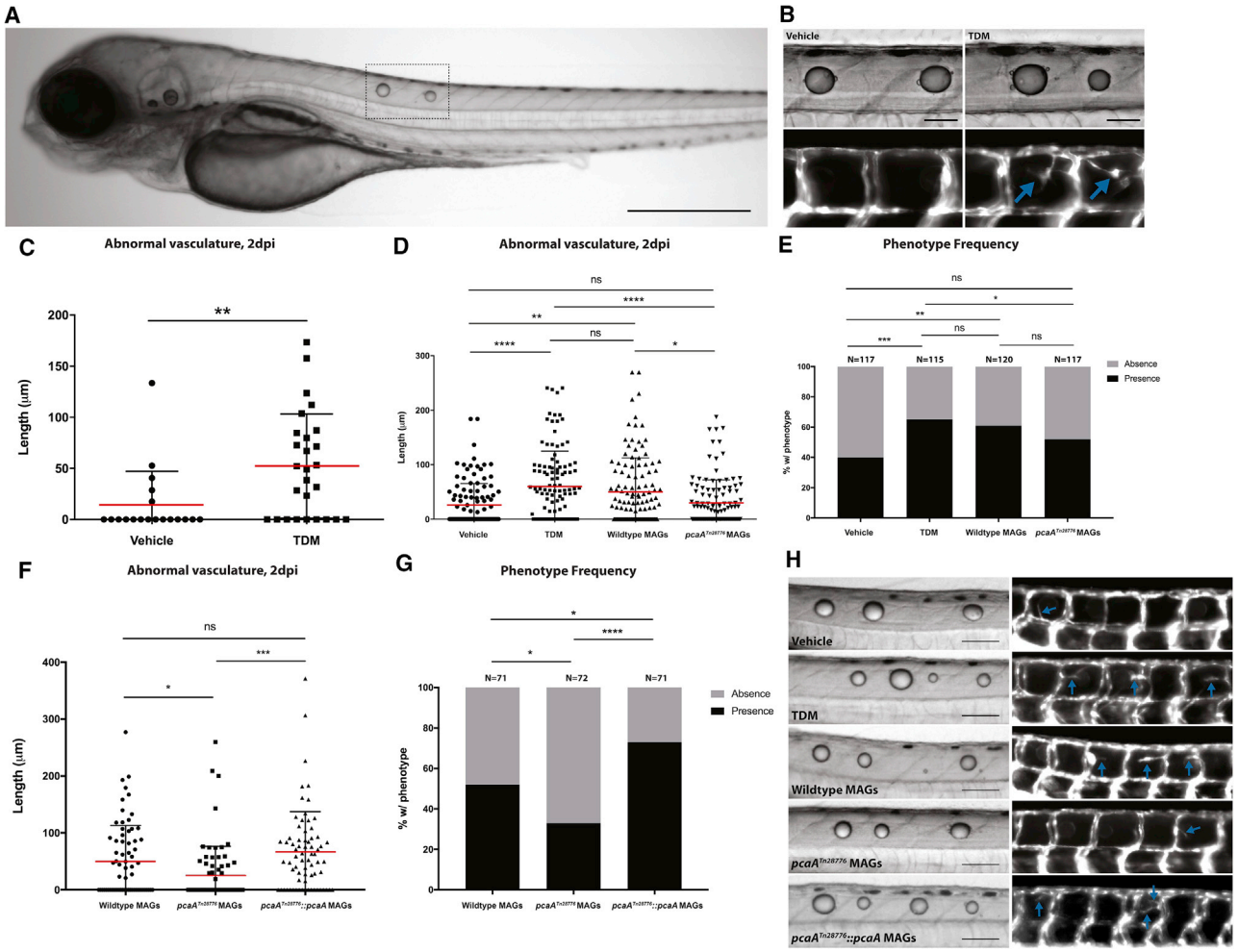

Figure 2. Purified TDM and Mycolic Acid Glycolipids from Wild-Type Bacteria but Not *pcaA* Mutants Elicit Robust Angiogenesis

(A) Representative image of 2-day post-injection larvae injected dorsally with TDM. Dotted line indicates injection site and droplet coalescence. Scale bar, 500 μm.

(B) Representative images of injections of either vehicle (left) or TDM (right) into *Tg(kdrl:EGFP)* animals. Blue arrows indicate abnormal vasculature (lower panels). Scale bars, 100 μm.

(C) Quantification of abnormal vasculature induced by TDM or vehicle alone. Representative of three experiments. **p < 0.01, Student's t test.

(D) Quantification of abnormal vasculature induced by MAGs isolated from wild-type or *pcaA* mutant *M. marinum*, with vehicle alone and TDM as negative and positive controls, respectively. Data from three experiments combined. *p < 0.05; **p < 0.01; ****p < 0.0001; one-way ANOVA with Tukey's multiple comparison post-test.

(E) Frequency of presence or absence of abnormal vasculature. *p < 0.05; **p < 0.01; ***p < 0.001; Fisher's exact test.

(F) Quantification of the length of abnormal vasculature induced by MAGs (5 mg/mL) isolated from $pcaA^{Tn28776}$:*pcaA*. MAGs from wild-type and $pcaA^{Tn28776}$ included as positive and negative controls. Data from three experiments combined. *p < 0.05; ***p < 0.001; one-way ANOVA with Tukey's multiple comparison post-test.

(G) Frequency of presence or absence of abnormal vasculature. *p < 0.05; ****p < 0.0001; Fisher's exact test.

(H) Representative images of larvae injected with vehicle, TDM, wild-type MAGs, MAGs isolated from $pcaA^{Tn28776}$, and MAGs isolated from $pcaA^{Tn28776}$:*pcaA*. Blue arrows indicate abnormal vasculature. Scale bars, 100 μm.

CRISPR/Cas9 knockouts of Myd88 and the two zebrafish FcRγ paralogs to abrogate most Toll-like receptor and Mincle/MCL signaling, respectively. Animals homozygous for a 22-bp deletion in Exon 1 *of* myd88 showed no differences in TDM-induced vascularization compared with heterozygous or wild-type siblings (Figures S3A–S3C). For the FcRγ experiments, we generated mosaic FcRγ knockout larvae in the *Tg(kdrl:EGFP)* background by CRISPR/Cas9 targeting of both FcRγ paralogs. Mosaic FcRγ knockout animals exhibited a significant decrease in abnormal vasculature in response to TDM compared with the control group (Figures S3D and S3E), suggesting that FcRγ contributes to TDM-induced angiogenesis.

Purified Mycolic Acid-Containing Glycolipids from Wild-Type but Not *pcaA* Mutant Bacteria Induce Angiogenesis

We next sought to determine if the different TDM compositions present within the cell walls of wild-type and *pcaA* mutant *M. marinum* were responsible for differences in the *in vivo*

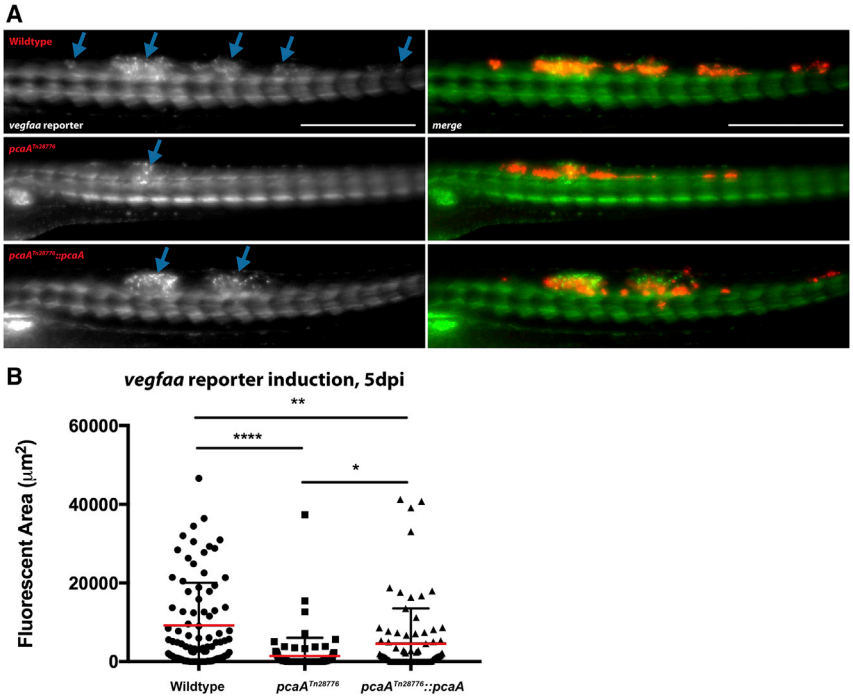

Figure 3. *pcaA* Mutants Fail to Induce Host *vegfaa* Reporter Expression

(A and B) Representative images of *TgBAC (vegfaa:EGFP)* larvae 5 dpi infected with either wild-type (top), *pcaA* mutant (middle), or complemented *pcaA* mutant *M. marinum* (bottom). Blue arrows denote areas of GFP signal above normal developmental pattern (A). Scale bars, 500 μm. Quantification of GFP signal above baseline for wild-type, *pcaA* mutant, and complemented *pcaA* mutant larval infections. Data from three experiments combined. *$p < 0.05$; **$p < 0.01$; ****$p < 0.0001$; one-way ANOVA with Tukey's multiple comparison post-test. n = 88 for wild-type infections; n = 86 for *pcaA* mutant; n = 86 for complemented mutant (B).

angiogenic potential between strains. We isolated free mycolic acid-containing glycolipids (MAGs), which in mycobacteria consist primarily of TDM (Bloch et al., 1953), from wild-type and *pcaA* mutant *M. marinum* by overnight extraction with 2:1 chloroform:methanol followed by precipitation in acetone (Parish and Stoker, 2001).

Resolution of the TDM species in the *pcaA* mutant by TLC revealed a reduced proportion of alpha-mycolate-containing TDM relative to keto- and methoxy-mycolate TDM in the *pcaA* mutant relative to wild-type (Figures S1A and S1B). Similarly, the *M. tuberculosis pcaA* knockout exhibits a large reduction in the proportion of alpha-mycolate-containing TDM (Glickman et al., 2000; Rao et al., 2005).

To confirm that *M. marinum* PcaA possesses the same enzymatic function as the *M. tuberculosis* and *M. bovis* orthologs, we isolated MAMEs from wild-type and *pcaA* mutant *M. marinum*. Resolution of this fraction by TLC again revealed a reduced proportion of alpha-mycolate MAMEs compared with the methoxy/keto fraction (Figures S1C and S1D). Importantly, ^{1}H nuclear magnetic resonance on the alpha-mycolate fractions showed a 12-fold reduction in *cis*-cyclopropanation for MAMEs isolated from the *pcaA* mutant (Figures S1E and S1F). These results indicate both that *M. marinum* PcaA performs the same function as in other mycobacteria and that the transposon insertion produces a loss-of-function allele.

We then compared the *in vivo* angiogenic activity of wild-type purified MAGs with those isolated from the *pcaA* mutant and complemented mutant strains. Using the droplet administration method developed earlier, we injected equivalent doses of the purified MAGs from each strain into separate groups of larvae. MAGs from wild-type and complemented mutant bacteria consistently induced angiogenesis at a level equivalent to purified TDM, whereas this fraction from the *pcaA* mutant failed to induce angiogenesis above the vehicle control (Figures 2D–2H). The purified TDM control, wild-type MAGs, and complemented mutant MAGs all also exhibited an increase in the frequency at which abnormal vascularization was observed compared with either vehicle alone or mutant MAGs (Figures 2E and 2G). Thus, loss of *cis*-cyclopropyl-modified mycolic acids abrogates the ability of these lipids to induce robust angiogenesis *in vivo*.

pcaA Mutants Fail to Induce Vegfa Expression

We have previously demonstrated that the Vegf receptor ligand Vegfaa is induced around sites of infection with wild-type *M. marinum* (Oehlers et al., 2015). VEGFA has been reported to be expressed in human granuloma macrophages, where extensive vascularization also occurs (Datta et al., 2015). Given the requirement and sufficiency of cyclopropanated TDM for granuloma-associated angiogenesis, we hypothesized that the non-modified TDM present in *pcaA* mutants might fail to induce Vegfaa. We utilized a transgenic line in which *vegfaa* regulatory sequences direct expression of an EGFP reporter transgene (*TgBAC(vegfaa:EGFP)*^{pd260} (Karra et al., 2018). During larval development the *vegfaa* reporter is driven in the developing vasculature at low levels in a stereotyped pattern throughout the animal (Karra et al., 2018). However, larvae infected with wild-type bacteria exhibited robust activation of this reporter at the granuloma (Figures 3A and 3B). In contrast, larvae infected with *pcaA* mutant bacteria largely failed to induce any robust signal above the developmental expression level, despite the formation of well-structured granulomas (Figures 3A and 3B). Larvae infected with the complemented mutant strain exhibited an intermediate phenotype, with ~3-fold greater reporter induction on average compared with the mutant strain (Figures 3A and 3B). These data implicate PcaA-dependent chemical modification of TDM in specifically promoting Vegfaa activation within the granuloma and suggest that TDM-dependent angiogenesis proceeds through engagement of the canonical pro-angiogenic Vegf signaling pathway.

Previous characterization of the *M. tuberculosis pcaA* knockout strain in the murine model revealed a reduced host

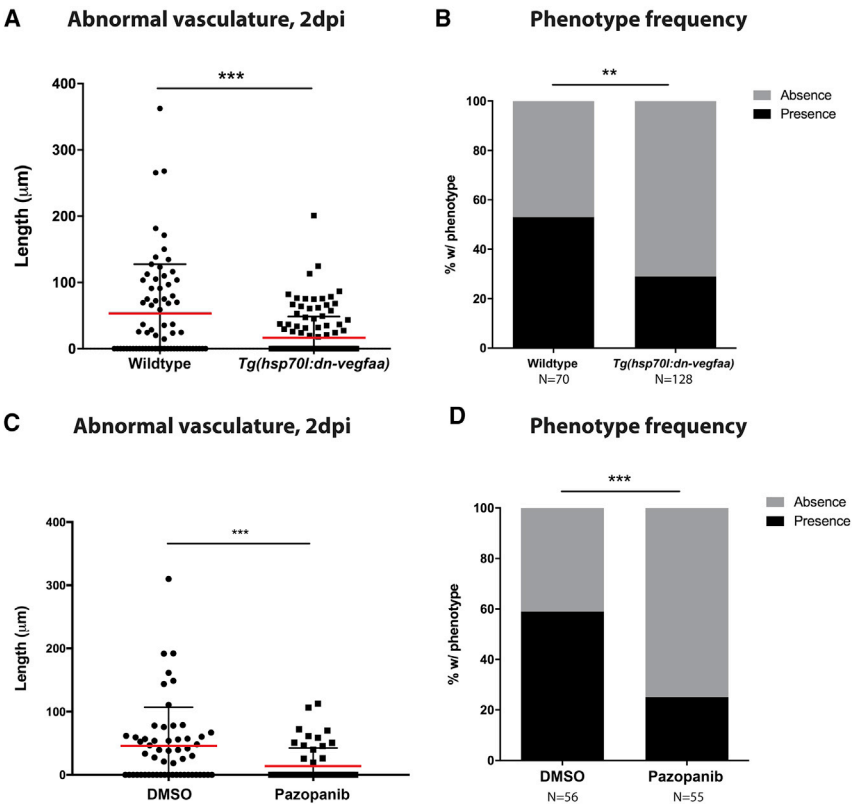

Figure 4. Inducible and Pharmacological Blockade of Vegf Pathway Activation Abrogates TDM-Induced Angiogenesis

(A) Quantification of abnormal vasculature at 2 dpi for larvae with and without the *Tg(hsp70l:dn-vegfaa)* transgene. ***p < 0.001, Student's t test.

(B) Comparison of the frequency of the presence or absence of abnormal vasculature between larvae with or without the *Tg(hsp70l:dn-vegfaa)* transgene after blinded scoring. Data from three experiments combined. **p < 0.01, Fisher's exact test.

(C) Quantification of abnormal vascularization at 2 dpi for larvae treated with either the pan-Vegf receptor inhibitor Pazopanib (250 nm) or vehicle (0.1% DMSO). ***p < 0.001, Student's t test.

(D) Phenotype frequency for vehicle- and Pazopanib-treated groups. Data from three experiments combined. ***p < 0.001, Fisher's exact test.

tumor necrosis factor (TNF) response during early infection (Rao et al., 2005). As the timing of Vegf induction occurs near the timing of the murine host TNF deficit, we wondered whether a reduced TNF response might play a role in the lack of angiogenesis in *pcaA* mutant infections. We first utilized the *tnfa* transcriptional reporter transgenic line *TgBAC(tnf:GFP)*^{pd1028} (Marjoram et al., 2015). We infected these larvae with wild-type, *pcaA* mutant, or complemented mutant *M. marinum*, and assessed the bacterial burden and GFP signal for each larva at 3 dpi. We found that there were no differences on average in GFP signal or relative TNF transcript levels among each group (Figures S4A–S4D).

To test functionally whether TNF signaling plays a role in Vegf pathway activation during infection, we generated mosaic CRISPR/Cas9 knockouts of TNF receptors 1 and 2 in *TgBAC (vegfaa:EGFP)* larvae. After infection with *M. marinum* we assessed bacterial burdens and GFP signal in the *vegfaa* reporter line at 5 dpi for each group. In TNF receptor-edited animals, bacterial burden was increased (Figure S4F), consistent with previous reports (Clay et al., 2008), and suggesting that the edited animals were indeed functionally deficient in TNF signaling. However, no differences were observed in *vegfaa* reporter signal between the two groups (Figures S4E and S4G). Thus, the *pcaA*-dependent *vegfaa* induction appears to be independent of TNF signaling.

Genetically Encoded, Inducible Blockade of Vegf Signaling Abrogates TDM-Induced Angiogenesis

We next tested whether TDM-induced angiogenesis was functionally dependent on Vegf signaling *in vivo*. We utilized a validated transgenic zebrafish line in which a heat shock-inducible promoter drives a dominant-negative form of Vegfaa (*Tg(hsp70l:dn-vegfaa)*^{bns100}), enabling temporally controlled inhibition of Vegf signaling (Marin-Juez et al., 2016). This dominant-negative form of Vegfaa functions by promoting the formation of an inactive heterodimer of native Vegfaa and dn-Vegfaa incapable of inducing Vegfr2 dimerization and subsequent pro-angiogenic signaling (Muller et al., 1997; Rossi et al., 2016).

To test a requirement for Vegf induction in TDM-induced angiogenesis, *Tg(hsp70l:dn-vegfaa);Tg(kdrl:EGFP)* larvae were heat shocked immediately prior to TDM injection at 2 dpf and heat shocked again at 3 dpf, followed by imaging at 4 dpf. Larvae were genotyped post hoc to distinguish dominant-negative *vegfaa*-expressing larvae from wild-type siblings. Animals expressing dominant-negative *vegfaa* showed dramatically reduced TDM-induced angiogenesis compared with heat-shocked wild-type siblings (Figures 4A and 4B). Thus, targeted genetic inhibition of Vegf is sufficient to abrogate TDM-induced angiogenesis.

To further validate these findings, we utilized a known small-molecule pan-Vegf receptor inhibitor, Pazopanib, which has been previously shown to effectively inhibit Vegf-dependent angiogenesis in humans and zebrafish (Oehlers et al., 2015; Podar et al., 2006). We injected *Tg(kdrl:EGFP)* larvae with TDM at 2 dpf, and randomly sorted half of the injected larvae into either E3 media containing vehicle (0.1% DMSO final concentration) or 250 nM Pazopanib. Similar to the heat shock-induced expression of dn-Vegfaa, treatment with Pazopanib abrogated the ability of TDM to induce angiogenesis *in vivo* (Figures 4C and 4D).

Wild-Type *M. marinum* Growth Advantage Begins with the Onset of Angiogenesis

To examine the link between compromised angiogenesis and reduced bacterial growth, we temporally assessed *pcaA* mutant growth deficiency relative to wild-type infection. Larvae were

infected with equal initial burdens of either wild-type, *pcaA* mutants, or the PcaA-complemented strain, and infection burdens were assessed at 1, 3, 4, and 5 dpi. Angiogenesis typically coincides with the beginning of granuloma formation at 3–4 dpi (data not shown). We observed identical *in vivo* growth among all three bacterial strains between days 1 and 3, suggesting that altered TDM does not lead to early differences in the ability of macrophages to restrict infection (Figures 5A and 5C). Instead, the *pcaA* mutant growth defect emerged only later, at 4 dpi, and became more pronounced at 5 dpi relative to wild-type (Figures 5A and 5C).

In addition, we used qRT-PCR to assess relative *M. marinum* 16S rRNA content from total RNA isolated from each group of larvae. The relative differences in burden among the three groups using this method were nearly identical to relative differences measured via fluorescent area (Figure S5G). This *pcaA*-dependent growth defect coincided with the observed decreased vascularization in the *pcaA* mutant at 4 dpi (Figure 5B). The burden and angiogenesis differences could be rescued by constitutive bacterial expression of PcaA (Figures 5A–5C). Taken together, these findings suggest that the loss of *pcaA*-dependent angiogenesis at 4 dpi may underlie the growth defect observed in *pcaA* mutant mycobacteria.

While these data suggested that reduced angiogenesis preceded reduced burden in *pcaA* mutants, we next probed more definitively whether reduced angiogenesis underlies the burden decreases in *pcaA* mutants. Taking advantage of the natural variability in zebrafish larval infections, we had previously found that wild-type *M. marinum* infection burden and infection-induced vascularization are positively correlated (Oehlers et al., 2015). We observed the same correlation of burden and vascularization for infections with wild-type or complemented *pcaA* mutant bacteria (Figures S5A and S5C), but no correlation between burden and angiogenesis for the *pcaA* mutant strain (Figure S5B). These results suggested that even high *pcaA* mutant burdens do not trigger robust angiogenesis.

Similarly, we compared levels of angiogenesis within the subset of data for which *pcaA* mutants and wild-type bacteria could be burden matched. Even under these constraints, *pcaA* mutant infections were severely compromised for angiogenesis compared with both wild-type and complemented strains (Figures S5D–S5F). Together, these analyses support a cause-and-effect relationship in which the *pcaA* mutant *in vivo* growth defect is downstream of an inability to induce robust granuloma vascularization.

Bacterial *pcaA* Mutant Deficits Are Non-cell Autonomous

To further probe the relationship between vascularization and burden, we reasoned that co-infection of differentially labeled wild-type and *pcaA* mutants would enable us to distinguish bacterium cell-autonomous effects of the mutation (for example, any compromised fitness arising from alterations of bacterial cell wall structure) from non-cell-autonomous effects relating to alterations in overall host environment. We co-infected animals with wild-type *M. marinum* in one color and *pcaA* mutants in a second color, and monitored the growth of each strain independently. We found that wild-type *M. marinum* could rescue both the *pcaA* angiogenesis and burden deficits in co-infected granulomas (Figures 5D–5F), further corroborating a principal role for non-cell-autonomous processes such as angiogenesis as the basis for the *pcaA* phenotype.

PcaA Mutants Exhibit a Growth Defect as a Result of a Failure to Engage the Vegf Pathway

Based on these data and *in vivo* imaging of the *vegfaa* reporter, we hypothesized that the loss of vascularization and restricted growth in the *pcaA* mutant resulted from a failure of Vegf-dependent vascularization. We infected *Tg(kdrl:EGFP)* and *Tg(kdrl:EGFP);Tg(hsp70l:dn-vegfaa)* larvae with wild-type or *pcaA* mutant *M. marinum*, heat shocked once a day at 3 and 4 dpi, and analyzed bacterial burden and vasculature at 5 dpi. In animals infected with wild-type *M. marinum*, we found that, as expected, there was a significant reduction in both angiogenesis (Figure 6B) and bacterial burden for the induced transgenic larvae (Figures 6A and 6C). Although small-molecule- and antibody-based manipulation of this pathway has been reported previously in mycobacterial infection (Datta et al., 2015; Oehlers et al., 2015), these results provide direct genetic evidence that inhibition of Vegf signaling is host-beneficial in early mycobacterial infection.

In contrast, inducible inhibition of Vegfaa signaling in the *pcaA* mutants had no effect on burden (Figure 6A). Thus, *in vivo*, the entirety of physiologically relevant Vegf production during early infection is *pcaA* dependent. Consistent with the requirement for *pcaA* in Vegf induction, the infection burden in dn-Vegfaa larvae infected with wild-type bacteria was reduced to the level seen in the *pcaA* mutant infections. These data demonstrate that Vegf pathway activation is a bacteria-beneficial host process for pathogenic mycobacteria during early infection and provide additional evidence that the defects observed for the *pcaA* mutant derive from its inability to activate the Vegf pathway and vascularize infection foci.

DISCUSSION

Pathogenic mycobacteria are capable of both evading the host immune response and reprogramming host phagocytes in order to modify their environment. It is known that granulomas formed during *M. tuberculosis* infection initially become highly vascularized, and this angiogenesis has been shown to facilitate bacterial growth, likely by mitigating hypoxia and nutrient deprivation within the granuloma interior and promoting dissemination (Aly et al., 2007; Oehlers et al., 2015; Tsai et al., 2006; Ulrichs et al., 2005). Previous work found that granuloma angiogenesis is macrophage dependent, and host-directed chemical inhibition of Vegf signaling abrogates vessel growth and reduces bacterial fitness (Oehlers et al., 2015), implying that pathogenic mycobacteria may drive or enhance this process within the host.

Here, we leveraged the unique advantages of the zebrafish model to demonstrate that specific chemical modifications to mycolic acids, a unique class of lipids constituting the major component of the outer cell wall of mycobacteria, are largely responsible for the early vascularization of infection foci. Specifically, we found that proximal *cis*-cyclopropanation of the mycolic acid tails of TDM is the major angiogenic component of mycolic acid-containing cell wall lipids. This modification has previously been reported to play a role in interactions with

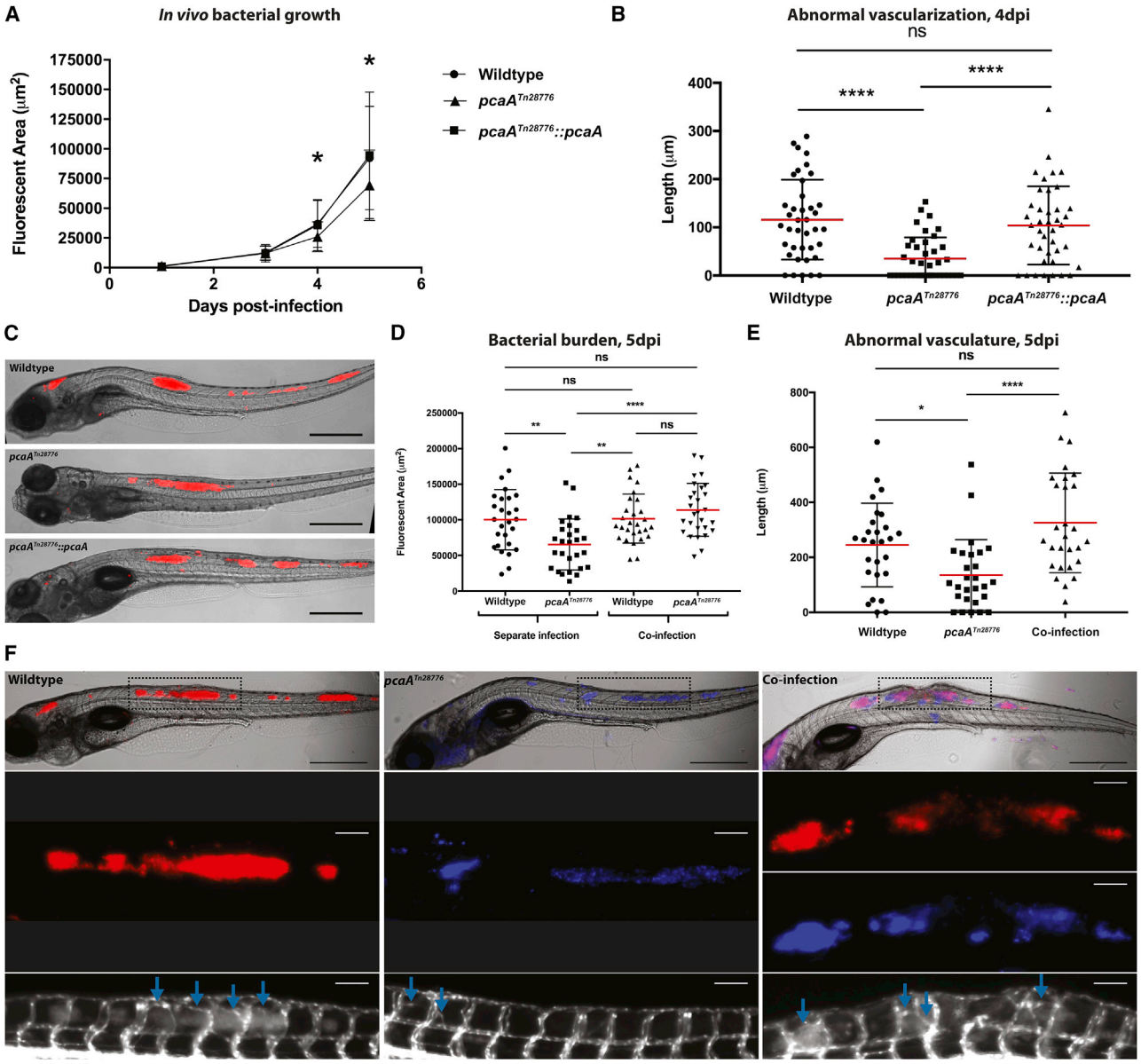

Figure 5. pcaA Mutant Bacteria Exhibit *In vivo* Growth Defects Coinciding with Onset of Granuloma Angiogenesis

(A) Five-day time course of larvae infected with wild-type, *pcaA* mutant, or complemented mutant *M. marinum* strains. Bacterial burdens were measured at 1, 3, 4, and 5 dpi. At 4 dpi *pcaA* mutants exhibit a reduced growth rate, which persists through 5 dpi. The complemented mutant strain exhibits wild-type levels of growth throughout. Representative of three independent experiments. *$p < 0.05$; one-way ANOVA with Dunnett's multiple comparison post-test. n = 40 for each group.

(B) Quantification of abnormal vascularization. The timing of the growth defect correlates with the onset of robust vascularization for wild-type and complemented strain infections but a failure to extensively vascularize infection foci for *pcaA* mutant strain infections. ****$p < 0.0001$; one-way ANOVA with Tukey's multiple comparison post-test. n = 40 for each group.

(C) Representative images of larvae at 5 dpi infected with each of the *M. marinum* strains. Wild-type, upper panel; *pcaA* mutant, middle; complemented mutant, lower. Scale bars, 500 μm.

(D–F) Larvae possessing the *Tg(kdrl:EGFP)* transgene were co-infected with wild-type and PcaA mutant *M. marinum*. Bacterial burden (D) and length of abnormal vasculature (E) were quantified for each larva at 5 dpi. *$p < 0.05$; **$p < 0.01$; ****$p < 0.0001$; one-way ANOVA with Tukey's multiple comparison post-test. Data shown represent an aggregate of two independent experiments. n = 27 for wild-type infections alone; n = 27 for *pcaA* mutant infections alone; n = 28 for co-infection. (F) Representative images of each infection. Upper panels: merge of bright-field and fluorescent channels. Red depicts wild-type *M. marinum*; blue depicts *pcaA* mutant *M. marinum*; purple depicts co-localization between the two strains. Dotted lines denote the area shown in lower panels. Scale bars, 500 μm. Middle panels: fluorescent channels alone, showing infection burden. Lower panels: vasculature. Blue arrows denote intersegmental vessel growth characteristic of granuloma angiogenesis. Scale bars, 100 μm.

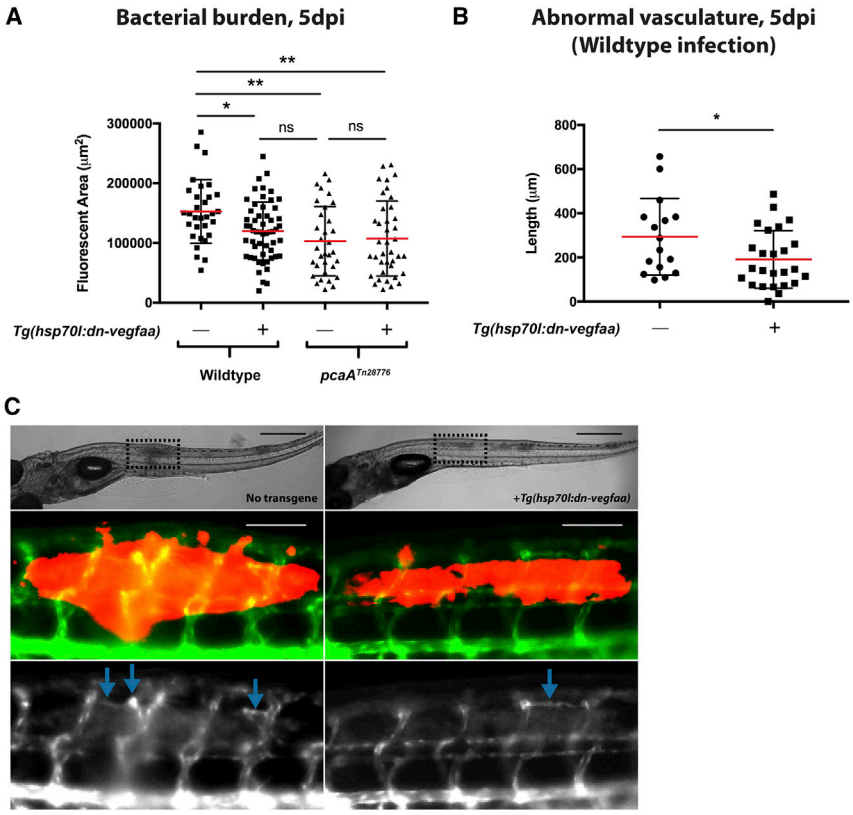

Figure 6. Vegf Pathway Blockade Inhibits *In Vivo* Growth of Wild-Type but Not *pcaA* Mutants

(A) Bacterial burden of larvae with or without the *Tg(hsp70l:dn-vegfaa)* transgene at 5 dpi, infected with either wild-type or *pcaA* mutant *M. marinum*. Expression of the transgene induces a reduction in wild-type *M. marinum* burden compared with larvae without the transgene. Expression of the transgene had no effect on the bacterial burdens of larvae infected with the PcaA mutant strain. *p < 0.05; **p < 0.01; one-way ANOVA with Tukey's multiple comparison post-test. n = 31 and n = 55 for wild-type infections in larvae without or with the *Tg(hsp70l:dn-vegfaa)* transgene, respectively; n = 33 and n = 39 for *pcaA* mutant infections in larvae without or with the *Tg(hsp70l:dn-vegfaa)* transgene, respectively.

(B) Quantification of abnormal vasculature during wild-type infections for *Tg(kdrl:EGFP)*$^{+}$ larvae with or without the *Tg(hsp70l:dn-vegfaa)* transgene. The double transgenic larvae were present as a subset of the cross between the *Tg(kdrl:EGFP)* and *Tg(hsp70l:dn-vegfaa)* transgenic lines. Induction of the *Tg(hsp70l:dn-vegfaa)* transgene results in a reduction in infection-induced angiogenesis. *p < 0.05, Student's t test. n = 16 and n = 25 for larvae without or with the *Tg(hsp70l:dn-vegfaa)* transgene, respectively.

(C) Representative images of vascularization in larvae with the *Tg(hsp70l:dn-vegfaa)* transgene (right panels) and without (left panels). Upper panels: bright field, with the dotted line depicting regions shown in the lower panels. Scale bars, 500 μm. Middle panels: merge of vasculature and infection. Lower panels: vasculature alone. Scale bars, 100 μm. All quantitation performed blind to genotype.

innate immune cells, but its role in angiogenesis had not been examined (Glickman et al., 2000; Rao et al., 2005).

Loss of these *cis*-cyclopropanated lipids during infection leads to a reduced overall bacterial burden that coincides with the normal onset of granuloma vascularization. The *in vivo* pathogen growth deficiency during this period appears to be largely if not entirely driven by a defect in Vegf pathway activation after granuloma formation. VEGFA induction in granuloma macrophages has consistently been reported to be a feature of mycobacterial infection in non-human primates and in humans (Datta et al., 2015; Matsuyama et al., 2000; Polena et al., 2016). Similarly, in zebrafish, Vegfaa production arises in granuloma macrophages, and angiogenesis is macrophage dependent (Oehlers et al., 2015). Here, using transgenic lines, we found that Vegfaa production arises at the granuloma in a *pcaA*-dependent fashion, and that selective genetic inhibition of Vegfaa signaling alone reduces bacterial burden to *pcaA* mutant levels.

These data suggest that vascularization of mycobacterial granulomas is not merely a passive phenomenon driven by the host response to dense, hypoxic cell aggregates. Rather, pathogenic mycobacteria actively promote or accelerate angiogenesis, expending energy by chemically modifying a cell wall lipid in a manner that, while not essential for viability, nonetheless creates a significant growth advantage *in vivo*.

TDM engages multiple host pathways that may promote mycobacterial pathogenesis, and thus the molecule may induce pleiotropic effects (Axelrod et al., 2008; Hunter et al., 2006; Indrigo et al., 2003; Middlebrook et al., 1947; Patin et al., 2017; Sakamoto et al., 2013). Here, however, we find that one specific chemical modification drives TDM's angiogenic activity via Vegfaa induction. Importantly, the *pcaA* mutants were not defective for initial *in vivo* growth within macrophages over the first 3 days of infection, and burden defects coincided with differences in angiogenesis. No additional burden defects emerged in the *pcaA* mutants upon genetic blockade of Vegfaa signaling, suggesting that the physiologically relevant effects of Vegfaa during early mycobacterial infection may be entirely *pcaA* dependent.

In cell culture models and in mice, *M. tuberculosis pcaA* mutants were shown to induce less initial TNF and to have a growth deficit at 7 dpi, although there was recovery to wild-type bacterial numbers at later time points (Rao et al., 2005). However, the effects we have observed on angiogenesis are difficult to translate or probe in standard mouse models; C57Bl/6 mouse *M. tuberculosis* granulomas do not form the extensively structured hypoxic granulomas observed in human disease (Harper et al., 2012; Tsai et al., 2006).

The Vegf dependence of the wild-type growth advantage we observed in this study may be complementary to the previously observed TNF-dependent growth advantage (Rao et al., 2005).

Pathogenic angiogenesis possesses a complex relationship with TNF. Short TNF pulses early in inflammation can prime endothelial cells for sprouting and proliferation while simultaneously blocking Vegf signaling, delaying but ultimately promoting angiogenesis (Sainson et al., 2008). In our model, however, TNF signaling does not appear to be crucial for early Vegf induction. Other reported activities of TDM may also influence vascularization at the mycobacterial granuloma; TDM can induce macrophage expression of MMP9, which has been implicated in angiogenesis via mobilization of VEGF as well as granuloma formation (Bergers et al., 2000; Sakamoto et al., 2013; Volkman et al., 2010).

Triggering host angiogenesis at the outset of infection may provide a mechanism by which mycobacteria maximize growth prior to subsequent restriction by host immunity. By initiating angiogenesis, the pathogen not only increases the delivery of oxygen and nutrients, but also generates conduits through which it may spread to distal tissue sites to establish a multi-focal infection (Oehlers et al., 2015; Polena et al., 2016). We have shown here and previously that interception of the Vegf and other pro-angiogenic pathways can be used to limit mycobacterial growth during infection, including in adult, established infections (Oehlers et al., 2015, 2017). Thus, host components engaged by *cis*-cyclopropanated TDM upstream of Vegfaa induction are attractive targets for further study. A fuller understanding of host interactions with this specific mycobacterial lipid may yield druggable targets in the host that have the potential to synergize with current anti-tubercular therapies via modulation of granuloma vasculature.

STAR★METHODS

Detailed methods are provided in the online version of this paper and include the following:

- KEY RESOURCES TABLE
- CONTACT FOR REAGENT AND RESOURCE SHARING
- EXPERIMENTAL MODEL AND SUBJECT DETAILS
  - Zebrafish (Danio Rerio)
  - Mycobacterium Marinum
- METHOD DETAILS
  - Microinjection of M. marinum
  - Lipid Analysis
  - Generating TNFR1/TNFR2 Mosaic Knockout Larvae
  - Generating FcRγ Mosaic Knockout Larvae
  - Injection into Single Cell Embryos
  - Generating the myd88 Knockout Line
  - *Use of* Tg(hsp70l:dn-vegfaa) *Larvae*
  - *In vitro* Growth Analysis
  - RT-qPCR
  - Pazopanib Treatment
- QUANTIFICATION AND STATISTICAL ANALYSIS
  - Image Analysis
  - Statistics

SUPPLEMENTAL INFORMATION

Supplemental Information includes six figures and one table and can be found with this article online at https://doi.org/10.1016/j.chom.2018.09.004.

ACKNOWLEDGMENTS

We are grateful to S. Abraham, J. Coers, M. Kuehn, J. Rawls, and members of the Tobin laboratory for helpful discussions, C. Cosma and L. Ramakrishnan for the kind gift of the transposon mutants, and E. Hunt for fish care. This work was supported by an American Cancer Society Postdoctoral Fellowship PF-13-223-01-MPC (to M.R.C.); a Damon Runyon Postdoctoral Fellowship (to C.J.C.); a Vallee Scholar Award (D.M.T.); NIH grants AI130236 and AI125517 (to D.M.T.); AI051622 (to C.R.B.); and HL081674 (to K.D.P.); and the Max Planck Society (to D.Y.R.S.).

AUTHOR CONTRIBUTIONS

Conceptualization, E.M.W. and D.M.T.; Methodology, E.M.W., M.R.C., C.J.C., A.R., M.M., M.D.F., K.D.P., D.Y.R.S., C.R.B., and D.M.T.; Investigation, E.M.W., M.R.C., C.J.C., and W.J.B.; Writing – Original Draft, E.M.W. and D.M.T.; Writing – Review & Editing, E.M.W., M.R.C., C.J.C., A.R., M.M., M.D.F., W.J.B., K.D.P., D.Y.R.S., C.R.B., and D.M.T.; Funding Acquisition, M.R.C., C.J.C., K.D.P., D.Y.R.S., C.R.B., and D.M.T.; Resources, E.M.W., A.R., M.M., M.D.F., K.D.P., and D.Y.R.S. Supervision, K.D.P., D.Y.R.S., C.R.B., and D.M.T.

DECLARATION OF INTERESTS

The authors declare no competing interests.

Received: April 23, 2018
Revised: August 6, 2018
Accepted: September 6, 2018
Published: October 10, 2018

REFERENCES

Aly, S., Laskay, T., Mages, J., Malzan, A., Lang, R., and Ehlers, S. (2007). Interferon-gamma-dependent mechanisms of mycobacteria-induced pulmonary immunopathology: the role of angiostasis and CXCR3-targeted chemokines for granuloma necrosis. J. Pathol. *212*, 295–305.

Axelrod, S., Oschkinat, H., Enders, J., Schlegel, B., Brinkmann, V., Kaufmann, S.H., Haas, A., and Schaible, U.E. (2008). Delay of phagosome maturation by a mycobacterial lipid is reversed by nitric oxide. Cell. Microbiol. *10*, 1530–1545.

Barry, C.E., 3rd, Lee, R.E., Mdluli, K., Sampson, A.E., Schroeder, B.G., Slayden, R.A., and Yuan, Y. (1998). Mycolic acids: structure, biosynthesis and physiological functions. Prog. Lipid Res. *37*, 143–179.

Bergers, G., Brekken, R., McMahon, G., Vu, T.H., Itoh, T., Tamaki, K., Tanzawa, K., Thorpe, P., Itohara, S., Werb, Z., et al. (2000). Matrix metalloproteinase-9 triggers the angiogenic switch during carcinogenesis. Nat. Cell Biol. *2*, 737–744.

Bloch, H., Sorkin, E., and Erlenmeyer, H. (1953). A toxic lipid component of the tubercle bacillus (cord factor) .1. Isolation from petroleum ether extracts of young bacterial cultures. Am. Rev. Tuberc. Pulm. *67*, 629–643.

Bowdish, D.M., Sakamoto, K., Kim, M.J., Kroos, M., Mukhopadhyay, S., Leifer, C.A., Tryggvason, K., Gordon, S., and Russell, D.G. (2009). MARCO, TLR2, and CD14 are required for macrophage cytokine responses to mycobacterial trehalose dimycolate and *Mycobacterium tuberculosis*. PLoS Pathog. *5*, e1000474.

Brennan, P.J. (2003). Structure, function, and biogenesis of the cell wall of *Mycobacterium tuberculosis*. Tuberculosis (Edinb) *83*, 91–97.

Brennan, P.J., and Besra, G.S. (1997). Structure, function and biogenesis of the mycobacterial cell wall. Biochem. Soc. Trans. *25*, 188–194.

Brennan, P.J., and Nikaido, H. (1995). The envelope of mycobacteria. Annu. Rev. Biochem. *64*, 29–63.

Chakravorty, S., Helb, D., Burday, M., Connell, N., and Alland, D. (2007). A detailed analysis of 16S ribosomal RNA gene segments for the diagnosis of pathogenic bacteria. J. Microbiol. Methods *69*, 330–339.

Clay, H., Volkman, H.E., and Ramakrishnan, L. (2008). Tumor necrosis factor signaling mediates resistance to mycobacteria by inhibiting bacterial growth and macrophage death. Immunity *29*, 283–294.

Cronan, M.R., Beerman, R.W., Rosenberg, A.F., Saelens, J.W., Johnson, M.G., Oehlers, S.H., Sisk, D.M., Jurcic Smith, K.L., Medvitz, N.A., Miller, S.E., et al. (2016). Macrophage epithelial reprogramming underlies mycobacterial granuloma formation and promotes infection. Immunity *45*, 861–876.

Daffe, M., Laneelle, M.A., and Lacave, C. (1991). Structure and stereochemistry of mycolic acids of *Mycobacterium marinum* and *Mycobacterium ulcerans*. Res. Microbiol. *142*, 397–403.

Datta, M., Via, L.E., Kamoun, W.S., Liu, C., Chen, W., Seano, G., Weiner, D.M., Schimel, D., England, K., Martin, J.D., et al. (2015). Anti-vascular endothelial growth factor treatment normalizes tuberculosis granuloma vasculature and improves small molecule delivery. Proc. Natl. Acad. Sci. USA *112*, 1827–1832.

Davis, J.M., Clay, H., Lewis, J.L., Ghori, N., Herbomel, P., and Ramakrishnan, L. (2002). Real-time visualization of mycobacterium-macrophage interactions leading to initiation of granuloma formation in zebrafish embryos. Immunity *17*, 693–702.

Dubnau, E., Chan, J., Raynaud, C., Mohan, V.P., Laneelle, M.A., Yu, K.M., Quemard, A., Smith, I., and Daffe, M. (2000). Oxygenated mycolic acids are necessary for virulence of *Mycobacterium tuberculosis* in mice. Mol. Microbiol. *36*, 630–637.

Ernst, J.D. (2012). The immunological life cycle of tuberculosis. Nat. Rev. Immunol. *12*, 581–591.

Folkman, J. (2002). Role of angiogenesis in tumor growth and metastasis. Semin. Oncol. *29*, 15–18.

Geisel, R.E., Sakamoto, K., Russell, D.G., and Rhoades, E.R. (2005). In vivo activity of released cell wall lipids of *Mycobacterium bovis* bacillus Calmette-Guerin is due principally to trehalose mycolates. J. Immunol. *174*, 5007–5015.

Glickman, M.S., Cahill, S.M., and Jacobs, W.R., Jr. (2001). The *Mycobacterium tuberculosis* cmaA2 gene encodes a mycolic acid trans-cyclopropane synthetase. J. Biol. Chem. *276*, 2228–2233.

Glickman, M.S., Cox, J.S., and Jacobs, W.R., Jr. (2000). A novel mycolic acid cyclopropane synthetase is required for cording, persistence, and virulence of *Mycobacterium tuberculosis*. Mol. Cell *5*, 717–727.

Harding, J., Ritter, A., Rayasam, A., Fabry, Z., and Sandor, M. (2015). Lymphangiogenesis is induced by mycobacterial granulomas via vascular endothelial growth factor receptor-3 and supports systemic T-cell responses against mycobacterial antigen. Am. J. Pathol. *185*, 432–445.

Harper, J., Skerry, C., Davis, S.L., Tasneen, R., Weir, M., Kramnik, I., Bishai, W.R., Pomper, M.G., Nuermberger, E.L., and Jain, S.K. (2012). Mouse model of necrotic tuberculosis granulomas develops hypoxic lesions. J. Infect. Dis. *205*, 595–602.

Hunter, R.L., Olsen, M., Jagannath, C., and Actor, J.K. (2006). Trehalose 6,6'-dimycolate and lipid in the pathogenesis of caseating granulomas of tuberculosis in mice. Am. J. Pathol. *168*, 1249–1261.

Indrigo, J., Hunter, R.L., Jr., and Actor, J.K. (2003). Cord factor trehalose 6,6'-dimycolate (TDM) mediates trafficking events during mycobacterial infection of murine macrophages. Microbiology *149*, 2049–2059.

Jin, S.W., Beis, D., Mitchell, T., Chen, J.N., and Stainier, D.Y. (2005). Cellular and molecular analyses of vascular tube and lumen formation in zebrafish. Development *132*, 5199–5209.

Karra, R., Foglia, M.J., Choi, W.Y., Belliveau, C., DeBenedittis, P., and Poss, K.D. (2018). Vegfaa instructs cardiac muscle hyperplasia in adult zebrafish. Proc. Natl. Acad. Sci. USA *115*, 8805–8810.

Kennerly, D.A. (1986). Improved analysis of species of phospholipids using argentation thin-layer chromatography. J. Chromatogr. *363*, 462–467.

Kumar, N.P., Banurekha, V.V., Nair, D., and Babu, S. (2016). Circulating angiogenic factors as biomarkers of disease severity and bacterial burden in pulmonary tuberculosis. PLoS One *11*, e0146318.

Lang, R. (2013). Recognition of the mycobacterial cord factor by Mincle: relevance for granuloma formation and resistance to tuberculosis. Front. Immunol. *4*, 5.

Liew, W.C., and Orban, L. (2014). Zebrafish sex: a complicated affair. Brief Funct. Genomics *13*, 172–187.

Liu, J., Barry, C.E., 3rd, Besra, G.S., and Nikaido, H. (1996). Mycolic acid structure determines the fluidity of the mycobacterial cell wall. J. Biol. Chem. *271*, 29545–29551.

Lobato-Pascual, A., Saether, P.C., Fossum, S., Dissen, E., and Daws, M.R. (2013). Mincle, the receptor for mycobacterial cord factor, forms a functional receptor complex with MCL and FcepsilonRI-gamma. Eur. J. Immunol. *43*, 3167–3174.

Marin-Juez, R., Marass, M., Gauvrit, S., Rossi, A., Lai, S.L., Materna, S.C., Black, B.L., and Stainier, D.Y. (2016). Fast revascularization of the injured area is essential to support zebrafish heart regeneration. Proc. Natl. Acad. Sci. USA *113*, 11237–11242.

Marjoram, L., Alvers, A., Deerhake, M.E., Bagwell, J., Mankiewicz, J., Cocchiaro, J.L., Beerman, R.W., Willer, J., Sumigray, K.D., Katsanis, N., et al. (2015). Epigenetic control of intestinal barrier function and inflammation in zebrafish. Proc. Natl. Acad. Sci. USA *112*, 2770–2775.

Matsuyama, W., Hashiguchi, T., Matsumuro, K., Iwami, F., Hirotsu, Y., Kawabata, M., Arimura, K., and Osame, M. (2000). Increased serum level of vascular endothelial growth factor in pulmonary tuberculosis. Am. J. Respir. Crit. Care Med. *162*, 1120–1122.

Middlebrook, G., Dubos, R.J., and Pierce, C. (1947). Virulence and morphological characteristics of mammalian tubercle bacilli. J. Exp. Med. *86*, 175–184.

Miyake, Y., Masatsugu, O.H., and Yamasaki, S. (2015). C-type lectin receptor MCL facilitates Mincle expression and signaling through complex formation. J. Immunol. *194*, 5366–5374.

Miyake, Y., Toyonaga, K., Mori, D., Kakuta, S., Hoshino, Y., Oyamada, A., Yamada, H., Ono, K., Suyama, M., Iwakura, Y., et al. (2013). C-type lectin MCL is an FcRgamma-coupled receptor that mediates the adjuvanticity of mycobacterial cord factor. Immunity *38*, 1050–1062.

Moreno-Mateos, M.A., Vejnar, C.E., Beaudoin, J.D., Fernandez, J.P., Mis, E.K., Khokha, M.K., and Giraldez, A.J. (2015). CRISPRscan: designing highly efficient sgRNAs for CRISPR-Cas9 targeting in vivo. Nat. Methods *12*, 982–988.

Muller, Y.A., Li, B., Christinger, H.W., Wells, J.A., Cunningham, B.C., and de Vos, A.M. (1997). Vascular endothelial growth factor: crystal structure and functional mapping of the kinase domain receptor binding site. Proc. Natl. Acad. Sci. USA *94*, 7192–7197.

Oehlers, S.H., Cronan, M.R., Beerman, R.W., Johnson, M.G., Huang, J., Kontos, C.D., Stout, J.E., and Tobin, D.M. (2017). Infection-induced vascular permeability aids mycobacterial growth. J. Infect. Dis. *215*, 813–817.

Oehlers, S.H., Cronan, M.R., Scott, N.R., Thomas, M.I., Okuda, K.S., Walton, E.M., Beerman, R.W., Crosier, P.S., and Tobin, D.M. (2015). Interception of host angiogenic signalling limits mycobacterial growth. Nature *517*, 612–615.

Pagan, A.J., and Ramakrishnan, L. (2018). The formation and function of granulomas. Annu. Rev. Immunol. *36*, 639–665.

Parish, T., and Stoker, N.G., eds. (2001). *Mycobacterium tuberculosis* Protocols. Methods in Molecular Medicine, *54* (Humana Press).

Patin, E.C., Geffken, A.C., Willcocks, S., Leschczyk, C., Haas, A., Nimmerjahn, F., Lang, R., Ward, T.H., and Schaible, U.E. (2017). Trehalose dimycolate interferes with FcgammaR-mediated phagosome maturation through Mincle, SHP-1 and FcgammaRIIB signalling. PLoS One *12*, e0174973.

Pirson, C., Jones, G.J., Steinbach, S., Besra, G.S., and Vordermeier, H.M. (2012). Differential effects of *Mycobacterium bovis* - derived polar and apolar lipid fractions on bovine innate immune cells. Vet. Res. *43*, 54.

Podar, K., Tonon, G., Sattler, M., Tai, Y.T., Legouill, S., Yasui, H., Ishitsuka, K., Kumar, S., Kumar, R., Pandite, L.N., et al. (2006). The small-molecule VEGF receptor inhibitor pazopanib (GW786034B) targets both tumor and endothelial cells in multiple myeloma. Proc. Natl. Acad. Sci. USA *103*, 19478–19483.

Polena, H., Boudou, F., Tilleul, S., Dubois-Colas, N., Lecointe, C., Rakotosamimanana, N., Pelizzola, M., Andriamandimby, S.F., Raharimanga, V., Charles, P., et al. (2016). *Mycobacterium tuberculosis* exploits the formation of new blood vessels for its dissemination. Sci. Rep. *6*, 33162.

Rao, V., Fujiwara, N., Porcelli, S.A., and Glickman, M.S. (2005). *Mycobacterium tuberculosis* controls host innate immune activation through cyclopropane modification of a glycolipid effector molecule. J. Exp. Med. *201*, 535–543.

Richardson, M.B., and Williams, S.J. (2014). MCL and Mincle: C-type lectin receptors that sense damaged self and pathogen-associated molecular patterns. Front. Immunol. *5*, 288.

Rittershaus, E.S., Baek, S.H., and Sassetti, C.M. (2013). The normalcy of dormancy: common themes in microbial quiescence. Cell Host Microbe *13*, 643–651.

Rossi, A., Gauvrit, S., Marass, M., Pan, L., Moens, C.B., and Stainier, D.Y.R. (2016). Regulation of Vegf signaling by natural and synthetic ligands. Blood *128*, 2359–2366.

Sainson, R.C.A., Johnston, D.A., Chu, H.C., Holderfield, M.T., Nakatsu, M.N., Crampton, S.P., Davis, J., Conn, E., and Hughes, C.C.W. (2008). TNF primes endothelial cells for angiogenic sprouting by inducing a tip cell phenotype. Blood *111*, 4997–5007.

Saita, N., Fujiwara, N., Yano, I., Soejima, K., and Kobayashi, K. (2000). Trehalose 6,6'-dimycolate (cord factor) of *Mycobacterium tuberculosis* induces corneal angiogenesis in rats. Infect. Immun. *68*, 5991–5997.

Sakamoto, K., Kim, M.J., Rhoades, E.R., Allavena, R.E., Ehrt, S., Wainwright, H.C., Russell, D.G., and Rohde, K.H. (2013). Mycobacterial trehalose dimycolate reprograms macrophage global gene expression and activates matrix metalloproteinases. Infect. Immun. *81*, 764–776.

Swaim, L.E., Connolly, L.E., Volkman, H.E., Humbert, O., Born, D.E., and Ramakrishnan, L. (2006). *Mycobacterium marinum* infection of adult zebrafish causes caseating granulomatous tuberculosis and is moderated by adaptive immunity. Infect. Immun. *74*, 6108–6117.

Stover, C.K., de la Cruz, V.F., Fuerst, T.R., Burlein, J.E., Benson, L.A., Bennett, L.T., Bansal, G.P., Young, J.F., Lee, M.H., Hatfull, G.F., et al. (1991). New use of BCG for recombinant vaccines. Nature *351*, 456–460.

Sydor, T., von Bargen, K., Hsu, F.F., Huth, G., Holst, O., Wohlmann, J., Becken, U., Dykstra, T., Sohl, K., Lindner, B., et al. (2013). Diversion of phagosome trafficking by pathogenic *Rhodococcus equi* depends on mycolic acid chain length. Cell. Microbiol. *15*, 458–473.

Takaki, K., Davis, J.M., Winglee, K., and Ramakrishnan, L. (2013). Evaluation of the pathogenesis and treatment of *Mycobacterium marinum* infection in zebrafish. Nat. Protoc. *8*, 1114–1124.

Tobin, D.M., and Ramakrishnan, L. (2008). Comparative pathogenesis of *Mycobacterium marinum* and *Mycobacterium tuberculosis*. Cell. Microbiol. *10*, 1027–1039.

Tsai, M.C., Chakravarty, S., Zhu, G., Xu, J., Tanaka, K., Koch, C., Tufariello, J., Flynn, J., and Chan, J. (2006). Characterization of the tuberculous granuloma in murine and human lungs: cellular composition and relative tissue oxygen tension. Cell. Microbiol. *8*, 218–232.

Uchida, D., Yamashita, M., Kitano, T., and Iguchi, T. (2002). Oocyte apoptosis during the transition from ovary-like tissue to testes during sex differentiation of juvenile zebrafish. J. Exp. Biol. *205*, 711–718.

Ulrichs, T., Kosmiadi, G.A., Jorg, S., Pradl, L., Titukhina, M., Mishenko, V., Gushina, N., and Kaufmann, S.H. (2005). Differential organization of the local immune response in patients with active cavitary tuberculosis or with nonprogressive tuberculoma. J. Infect. Dis. *192*, 89–97.

Volkman, H.E., Pozos, T.C., Zheng, J., Davis, J.M., Rawls, J.F., and Ramakrishnan, L. (2010). Tuberculous granuloma induction via interaction of a bacterial secreted protein with host epithelium. Science *327*, 466–469.

Werninghaus, K., Babiak, A., Gross, O., Holscher, C., Dietrich, H., Agger, E.M., Mages, J., Mocsai, A., Schoenen, H., Finger, K., et al. (2009). Adjuvanticity of a synthetic cord factor analogue for subunit *Mycobacterium tuberculosis* vaccination requires FcRgamma-Syk-Card9-dependent innate immune activation. J. Exp. Med. *206*, 89–97.

STAR★METHODS

KEY RESOURCES TABLE

REAGENT or RESOURCE	SOURCE	IDENTIFIER
Bacterial and Virus Strains		
M. marinum; wildype (M strain)	(Oehlers et al., 2015)	N/A
M. marinum; *pcaA*^{Tn28776}	This paper	N/A
M. marinum; *pcaA*^{Tn20324}	This paper	N/A
M. marinum; *pcaA*^{Tn28776}::*pcaA*	This paper	N/A
Chemicals, Peptides, and Recombinant Proteins		
Mycolic acid-containing glycolipids; *M. marinum* wildtype	This paper; (Parish and Stoker, 2001)	N/A
Mycolic acid-containing glycolipids; *M. marinum pcaA*^{Tn28776}	This paper; (Parish and Stoker, 2001)	N/A
Mycolic acid-containing glycolipids; *M. marinum pcaA*^{Tn28776}::*pcaA*	This paper; (Parish and Stoker, 2001)	N/A
M. bovis alpha-mycolate TDM	Sigma-Aldrich	T3034
M. tuberculosis H37Rv TDM	BEI Resources	NR-14844
M. tuberculosis H37Rv MAMEs	BEI Resources	NR-14854
Incomplete Freund's Adjuvant	Sigma-Aldrich	F5506
Pazopanib	Sigma-Aldrich	CDS023580
Critical Commercial Assays		
TRIzol Reagent	Thermo Fisher Scientific	15596026
Melt Doctor HRM Master Mix	Thermo Fisher Scientific	4415440
SYBR Green PCR Master Mix	Thermo Fisher Scientific	4367659
InFusion HD Cloning Kit	Takara	639646
MEGAShortscript T7 Transcription Kit	Thermo Fisher Scientific	AM1354
RNeasy Mini Kit	Qiagen	74104
Q5 DNA Polymerase 2x Master Mix	NEB	M0492L
Experimental Models: Organisms/Strains		
Zebrafish line *Tg(kdrl:EGFP)*^{s843}	(Jin et al., 2005)	s843
Zebrafish line *TgBAC(vegfaa:EGFP)*^{pd260}	(Karra et al., 2018)	pd260
Zebrafish line *TgBAC(tnf:GFP)*^{pd1028}	(Marjoram et al., 2015)	pd1028
Zebrafish line *Tg(hsp70l:dn-vegfaa)*^{bns100}	(Marin-Juez et al., 2016)	bsn100
Zebrafish mutant line *myd88*$^{+/xt29}$	This paper	
Oligonucleotides		
See Table S1		
Recombinant DNA		
pMsp12:mCerulean-KanR	This paper	N/A
pMV261	(Stover et al., 1991)	Addgene #3668 (sequence only)
pMV261-PcaA-KanR	This paper	N/A
pMCHP-KanR	This paper	N/A
Software and Algorithms		
High Resolution Melt Software v3.1	Thermo Fisher Scientific	A30150
GraphPad Prism 7	https://www.graphpad.com/scientific-software/prism/	N/A
7500 Fast Real Time PCR Software v2.3	Thermo Fisher Scientific	N/A

CONTACT FOR REAGENT AND RESOURCE SHARING

Further information and requests for resources should be directed to and will be fulfilled by the Lead Contact, David Tobin (david.tobin@duke.edu).

EXPERIMENTAL MODEL AND SUBJECT DETAILS

Zebrafish (Danio Rerio)

All zebrafish husbandry and experimental procedures were performed in accordance and compliance with policies approved by the Duke University Institutional Animal Care and Use Committee (protocol A122-17-05). Unless otherwise indicated, all zebrafish are derived from the wildtype AB strain.

Adult Zebrafish Housing

Adult zebrafish used to generate all the larvae used in this study were housed together by transgenic genotype in 3 or 10 L tanks. Water conditions are as follows: temperature: 28°C; conductivity: 600-700 μS (maintained with Instant Ocean Sea Salt); pH: 7.0-7.3 (maintained with sodium bicarbonate; Arm & Hammer Pure Baking Soda).

Larval Zebrafish

All larval zebrafish used in this study were euthanized on or before 8 dpf. At these ages, sex is indeterminate for zebrafish (Liew and Orban, 2014; Uchida et al., 2002), and so no distinctions between male and female are made in the studies presented here.

Larvae were maintained at a temperature of 28.5°C in 100 mm petri dishes in 40-50 ml of sterile E3 media (5 mM NaCl, 178 μM KCl, 328 μM $CaCl_2$, 400 μM $MgCl_2$) at a maximum density of 50 larvae per dish. In all cases, at 1 dpi larvae were transferred to E3 supplemented with 1-phenyl-2-thiourea (PTU, Sigma-Aldrich cat# P7629), final concentration 45 μg/ml) to arrest pigment development.

In all cases, anesthesia was performed with the addition of Tricaine (Sigma Aldrich, cat# E10521) to a final concentration of 160 μg/ml. Unless otherwise stated, larvae were anesthetized prior to any manipulation (i.e., moving between dishes, microinjection, live imaging, etc.). Time in anesthetic was limited to the minimum amount of time required to perform the desired manipulation.

Mycobacterium Marinum

Wildtype

All strains used are derived from the *M. marinum* M strain. The wildtype *M. marinum* strain, expressing the tdTomato fluorescent protein and Hygromycin B resistance genes, has been described previously (Oehlers et al., 2015). Culture of wildtype bacteria was carried out on either 7H10 agar supplemented with Middlebrook OADC growth supplement (10% v/v; Sigma-Aldrich cat# M0678) and 50 μg/ml Hygromycin B or liquid 7H9 media supplemented with Middlebrook OADC growth supplement (10% v/v), 0.05% Tween 80 (Sigma-Aldrich cat# P1754), and 50 μg/ml Hygromycin B. Liquid 7H9 media containing OADC and Tween 80 is referred to hereafter as 7H9 Complete.

Transposon Mutants

The two transposon mutants with disruptions in the *pcaA* ORF ($pcaA^{Tn20324}$ and $pcaA^{Tn28776}$) were identified from a sequenced library of *M. marinum* transposon mutants (C. Cosma and L. Ramakrishnan), and the previously identified insertion sites were confirmed by PCR and sequencing. Primers used were F primer (annealing upstream of the 5' end of the pcaA ORF): 5'-AAGCCCTGTGGAACA GAAAG-3'; R primer (annealing downstream of the 3' end of the pcaA ORF): 5'-ATCAAGCCAACACGCCTG-3'; and TnMarR3 (annealing within the transposon and directing amplification across the 3' junction with genomic DNA): 5'-ACAACAAAGCTCTCAC CAACCGTG-3'. The following primer pairs were used in separate reactions for each of the mutants as well as a no template control: F/TnMarR3; R/TnMarR3. Of the PCRs performed, amplicons were generated only from F/TnMarR3 using $pcaA^{Tn28776}$ template and R/TnMarR3 using $pcaA^{Tn20324}$ template. Sequencing of the amplicons using TnMarR3 confirmed disruptive insertions of the transposons into the *pcaA* ORFs of both strains.

Transposon mutants possessed the TnMar transposon, conferring resistance to Hygromycin B. Fluorescent transposon mutant strains were generated via electroporation (800 Ω, 25 μF, 2.5 kV, 0.2 cm gap) with plasmid msp12:mCerulean-KanR (a gift from L. Ramakrishnan, University of Cambridge), resulting in the expression of the mCerulean fluorescent protein and conferring resistance to Kanamycin. Culture of transposon mutant strains was carried out using the same media as with wildtype bacteria except for the addition of 20 μg/ml Kanamycin to the media.

Complementation of the $pcaA^{Tn28776}$ *Strain*

The *pcaA* open reading frame (ORF) was amplified from wildtype *M. marinum* genomic DNA (F primer: 5'-AATCACTTCG CAATGTCCGTCCAGCTCACG-3'; R primer: 5'-GTCGATCGTACGCTACTTCTCCAAAGTGAACTGA-3'). The pMV261-KanR plasmid (a gift from the Ramakrishnan lab) that contained the *M. tuberculosis groEL* promoter (referred to hereafter as *hsp60*) was amplified and linearized via inverse PCR (F primer: 5'-TAGCGTACGATCGACTGC-3'; R primer 5'-CATTGCGAAGTGATTCCTCC-3'). The two fragments were ligated together via InFusion (Clontech) producing a plasmid conferring resistance to Kanamycin with the *pcaA* ORF immediately downstream of the mycobacterial *hsp60* promoter (referred to hereafter as pMV261-PcaA-KanR).

A fragment containing the hsp60 promoter and *pcaA* ORF was amplified from pMV261-PcaA-KanR (F primer: 5'- TCTCAT CAACCGTGGAAATCTAGAGGTGACCACAACG-3'; R primer: 5'-TCCAGCCAGAAAGTGTTGTTGGCTAGCTGATCACC-3'). The entire msp12:mCerulean-KanR plasmid was amplified and linearized via inverse PCR (F primer: 5'- CACTTTCTGGCTGGAT GATG-3'; R primer: 5'-CCACGGTTGATGAGAGCT-3'). The two fragments were ligated together via Infusion (Clontech) producing a plasmid conferring Kanamycin resistance as well as mycobacteria-specific constitutive expression of both the mCerulean fluorescent protein (*msp12* promoter) and *M. marinum* PcaA (*hsp60* promoter), referred to hereafter as pMCHP-KanR.

pMCHP-KanR was electroporated into $pcaA^{Tn28776}$, resulting in a Kanamycin/Hygromycin B-resistant mutant strain overexpressing PcaA and mCerulean.

METHOD DETAILS

Microinjection of M. marinum

All strains were prepared for infection in the same manner, as described previously (Takaki et al., 2013). Bacteria were cultured at 33°C in 50 ml 7H9 complete with the appropriate antibiotic(s) without shaking. At OD600 of 0.5-0.6, cultures were collected by centrifugation at 4000 x g for 20 min. Cultures were washed 3x with dH_2O to remove all traces of antibiotic, and resuspended in 1 ml of Freezing 7H9 (7H9 supplemented with 10% v/v Middlebrook OADC). The concentrated suspension was centrifuged at 770 x g, and the unpelleted bacteria in the supernatant were transferred to a fresh tube. The pellet was then resuspended in 1 ml Freezing 7H9 using a syringe. Centrifugation, supernatant collection, and resuspension were repeated until all bacteria had been transferred to the new collection tube. The entire volume of collected supernatants was then filtered through a 5 μm nylon syringe filter, and centrifuged at 14,000 x g for 5 min. The pellet was resuspended in 0.5 ml of Freezing 7H9, and bacteria concentration was elucidated by averaging the count of fluorescent bacteria of several serial dilutions. The concentrate was adjusted to 5.0 x 10^8 bacteria/ml with Freezing 7H9, distributed into 5 μl aliquots, and stored at −80°C.

Infections with either wildtype, transposon mutant, or complemented mutant *M. marinum* were performed as described (Oehlers et al., 2015). Briefly, larvae at 2 dpf were anesthetized with Tricaine and injected with 100-200 fluorescent bacteria dorsally near the rostral/caudal midline.

Microinjection of TDM, MAMEs, and MAGs

TDM (Sigma Aldrich, cat# T3034, purified from *M. bovis*; or BEI Resources cat# NR-14844, purified from *M. tuberculosis* H37Rv) at 2 mg/ml in Incomplete Freund's Adjuvant (Sigma Aldrich, cat# F5506) was dissolved in 2:1 chloroform:methanol to generate stock solutions of 1 mg/ml and 250 μg/ml, respectively. MAMEs (BEI Resources cat# NR-14854, purified from *M. tuberculosis* H37Rv) was dissolved in 2:1 chloroform:methanol to generate a stock solution of 1mg/ml. MAGs purified from the various *M. marinum* strains used in this study were dissolved TDM and MAMEs were prepared for injection by evaporating a small volume of the stock solution under gentle airflow, and resuspending in and appropriate volume of IFA to achieve 2 mg/ml final concentration. Larvae at 2 dpf were anesthetized in Tricaine in E3 media and injected with approximately 10-20 nl of TDM/IFA or MAMEs/IFA (See Figure 1 for anatomical location). Control larvae were injected with the same volume of IFA alone. Larvae were then washed once in E3 and transferred to fresh E3 supplemented with PTU to continue arresting pigment development.

Purification of MAGs from M. marinum

Wildtype and *pcaA*^{Tn28776} *M. marinum* were first inoculated from freezer stocks into 3 ml of 7H9 Complete liquid media starter culture supplemented with 50 μg/ml Hygromycin B, and incubated at 33°C in static culture until late log phase (OD600 of 0.8-1). The *pcaA*^{Tn28776}::*pcaA* strain was grown under identical conditions except for the addition of 20 μg/ml Kanamycin. Cultures were spun down and resuspended in 1 ml fresh 7H9 Complete media, and added to 500 ml of 7H9 Complete with appropriate antibiotic(s). Cultures were grown at 33°C with gentle shaking until mid-log phase (OD600 of 0.5-0.7). Purification of mycolic acid-containing glycolipids was then performed separately for each culture, as described (Parish and Stoker, 2001). Briefly, bacteria were collected and washed 3x with dH_2O, resuspended in 10 ml 2:1 chloroform:methanol, and incubated at room temperature overnight in a sealed container with vigorous stirring. The crude extract was collected, spun down to pellet insoluble debris, and slowly added to 500 ml acetone at -20°C and incubated overnight. Precipitate was recovered by spinning at 20,000x g for 15 min at 4°C, discarding the supernatant and resuspending in 2 ml 2:1 choloform:methanol. The solvent was evaporated under gentle airflow, and recovered material was weighed on an analytical balance. Each preparation was then resuspended at 5 mg/ml in 2:1 chloroform:methanol.

Purification of MAMEs from M. marinum

M. marinum strains were cultured as previously described for the MAG isolations. Alpha MAMEs were isolated by preparative TLC using EMD Millipore TLC Silica Gel 60 (Thermo Fisher Scientific cat# M1057150001) from crude MAMEs extracts. Briefly, 10 mg of each crude extract were developed in 94:6 petroleum ether:ethyl acetate. The alpha band was isolated by scraping and dissolved in deuterated chloroform ($CDCl_3$).

Lipid Analysis

MAGs

TLC was performed on EMD Millipore TLC Silica Gel 60 (Thermo Fisher Scientific cat# M1057150001) as described (Pirson et al., 2012), with impregnation with 10% silver nitrate in water as described (Kennerly, 1986). Briefly, impregnation was carried out by submerging the TLC plate in the silver nitrate solution for 30 seconds. The plate was then allowed to dry at room temperature for 1 hour followed by baking at 50°C, 80°C, and 100°C in a stepwise fashion for 20min at the first two temperatures and 40 min at the last. Plates were then allowed to cool at room temperature for 20 min before use. 20 μg of lipid extract in methylene chloride was spotted on the plate and allowed to dry prior to running in a 100:14:0.8 chloroform:methanol:water solution. The plate was developed by submersion in a 10% sulfuric acid in methanol followed by charring. Plates were imaged using a Google Pixel camera.

MAMEs

TLC of the MAMEs isolates was performed in the same manner as for the MAG isolates, with the following exceptions. The isolates were developed 2x in 95:5 hexanes:ethyl acetate. ^{1}H NMR was performed at 500 MHz with the sample dissolved in $CDCl_3$.

Generating TNFR1/TNFR2 Mosaic Knockout Larvae

sgRNA Synthesis

Target sites within the tnfrsfa and tnfrsfb loci were identified using the sgRNA prediction tool at www.crisprscan.org (Moreno-Mateos et al., 2015). Single stranded DNA oligos used to generate the sgRNA transcription templates for the tnfrsfa and tnfrsfb targets were 5'-taatacgactcactataGGGCTGGACGAGGTCCCTATgttttagagctagaa-3' and 5'-taatacgactcactataGGTGCAATGCAGTACTGCTTgtttagagctagaa-3', respectively.

Double-stranded template assembly was performed via PCR using Q5 DNA Polymerase (NEB) with either of the above oligos and the constant tail oligo 5'-AAAAGCACCGACTCGGTGCCACTTTTTCAAGTTGATAACGGACTAGCCTTATTTTAACTTGCTATTTCTAGCTCTAAAAC-3'. Cycling parameters: 98°C, 1 min; 14 cycles of 98°C, 10s, 45°C, 30s; 72°C, 15s. 1μg of template was used in an *in vitro* transcription reaction using the MEGAShortscript T7 Transcription Kit per the manufacturer's instructions (Thermo Fisher Scientific cat# AM1354). sgRNAs were purified using RNeasy Mini Kit (Qiagen cat# 74104).

Injection into Single Cell Embryos

Single cell embryos of the *TgBAC(vegfaa:EGFP)* were injected with ~10nl of the following mixture: 800ng/ul Cas9 protein (IDT, cat#1074182), 300mM KCl, 265ng/μl sgRNA.

Assessment of Lesions at Target Loci

Genomic DNA was extracted from whole larvae at 5 dpi at the conclusion of the experiment in the same manner as described previously. 1ul of a 1/10 dilution of this extract was used as a template for HRMA using the MeltDoctor HRM Master Mix (Thermo Fisher Scientific) per the manufacturer's instructions. Primers for TNFR1: Forward – 5'-CTGCTATTTGCAGTTCACGAG-3'; Reverse – 5'-GGTCAATGTTCTGCTCAGAAAC-3'. Primers for TNFR2: Forward – 5'-CTCTTCTAGGGACTCGCTTG-3'; Reverse – 5'-GGACACTTGAAACAATTGGGA-3'. PCR and melt profile were performed using the 7500 Fast Real-Time PCR System (Thermo Fisher Scientific). Genotyping analysis was performed by HRM Software 3.0 (Thermo Fisher Scientific) (Figures S6A and S6B).

Generating FcRγ Mosaic Knockout Larvae

sgRNA Synthesis

Target sites within the *fcer1g* and *fcer1gl* loci were identified using crisprscan.org.

Single stranded DNA oligos used to generate the sgRNA transcription templates for the fcer1g and fcer1gl targets were 5'-taatacgactcactataGGCAGATGCGATGAGTCTGAgttttagagctagaa-3' and 5'-taatacgactcactataGGCGGGATCCTGATCGTTTAgttttagagctagaa-3', respectively. Templates were assembled in the same manner as for the TNFR sgRNA templates.

Injection into Single Cell Embryos

Tg(kdrl:EGFP) single cell embryos were injected with ~10nl of the following mixture: 800ng/ul Cas9 protein (IDT, cat#1074182), 300mM KCl, 265ng/μl sgRNA.

Assessment of Lesions at Target Loci

Genomic DNA was extracted from whole larvae at 2 dpi at the conclusion of the experiments in the manner previously described. HRMA was performed using the following primers: Primers for *fcer1g*: Forward – 5'- AACTTGTTGCTCAGTATGTTC-3'; Reverse – 5'-GACAGTGAGAACAATCCCATAG-3'. Primers for *fcer1gl*: Forward – 5'-GTTTCTCAGCTGCGCAACA-3'; Reverse – 5'-GATGCTCACCTTTAATCTGCAG-3'. PCR and melt profile were performed using the 7500 Fast Real-Time PCR System (Thermo Fisher Scientific). Genotyping analysis was performed by HRM Software 3.0 (Thermo Fisher Scientific) (Figures S6C and S6D).

Generating the myd88 Knockout Line

sgRNA Synthesis

Target sites within the *myd88* locus were identified using crisprscan.org.

Single stranded DNA oligos used to generate the sgRNA transcription templates for the *myd88* target was 5'-taatacgactcactataGGCGGCAGACTGGAGGACAGgttttagagctagaa-3'.

Templates were assembled in the same manner as described previously.

Injection into Single Cell Embryos

Tg(kdrl:EGFP) single cell embryos were injected with ~10nl of the following mixture: 800ng/ul Cas9 protein (IDT, cat#1074182), 300mM KCl, 265ng/μl sgRNA.

Identification of Frameshift Alleles

Adult zebrafish derived from the injected embryos were crossed to wildtype fish, and the progeny were assessed via HRMA as described previously. F primer: 5'-CCGAAAGAAACTGGGTCTGTTCC-3'; R primer: 5'- ACGAGTTTCCCAGTCCGTCA-3'. Larvae exhibiting lesions at the *myd88* target locus were further analyzed by sequencing, and an allele exhibiting a 22 base-pair deletion was identified. This deletion begins at amino acid 39 (of 284) and results in a frameshift and premature translation termination after 59 amino acids. F1 adult fish heterozygous for this allele were identified and pooled, and larvae used for the experiments requiring *myd88* knockouts were generated by crossing these F1 adults. The resulting progeny exhibited Mendelian ratios of homozygous wildtype, heterozygous mutant, and homozygous mutant alleles via HRMA (See group N values, Figures S3C; HRMA output S6E).

Use of Tg(hsp70l:dn-vegfaa) *Larvae*

Heat Shock Conditions

For experiments involving TDM: All larvae subjected to heat shock were incubated at 37°C for 75 min, occurring at -4 hrs and +20 hrs with respect to the time of TDM injection. For experiments involving infection: Heat shocks occurred at 3 and 4 dpi; 37°C for 75 min each time.

Genotyping

Genomic DNA was extracted individually from whole larvae as described previously. Extracts were diluted 1:10 and 1 μl from each larva was used as a template for PCR. Genotyping was carried out for up to 96 larvae in parallel using an Applied Biosystems 7500 Fast Real-Time PCR machine followed by High-Resolution Melt Analysis (HRMA) using MeltDoctor HRM Reagents (Thermo Fisher Scientific). A competitive pair of PCRs were performed concurrently, allowing expedited, automated identification of transgene-containing samples by melt curve analysis. Briefly, one forward primer (Primer F1; 5'-GAGAACGGTGTGACGGTAAC-3') anneals to the 3' end of Intron 2-3 in the endogenous *vegfaa* locus; another forward primer (Primer F2; 5'-CTGCCCACATACCCAAAGAAG-3') anneals to the 5' end of *vegfaa* Exon 2 in the endogenous locus and within the *dn-vegfaa* transgene; and a shared reverse primer (Primer R; 5'-GATGATGTCTACCAGCAGCTC-3') anneals within Exon 3 of both the endogenous locus and within the *dn-vegfaa* transgene. The resulting reaction generates different, highly reproducible amplicon pools depending on the presence/absence of the transgene, which can be distinguished by HRMA (Figure S6F). HRMA patterns were initially assigned to genotypes based on analysis of a subset of samples using a simple presence/absence PCR for the transgene followed by Agarose Gel Electrophoresis (F primer: 5'-CATGTG GACTGCCTATGTTCATC-3'; R primer: 5'-CTTCTTTGGGTATGTGGGCAG-3').

In vitro Growth Analysis

Starter cultures were generated by inoculating 1 ml 7H9 Complete with a stab of −80°C freezer stock of each strain tested. Starter cultures were allowed to grow to stationary phase. Bacteria were pelleted by centrifugation, and resuspended in 1 ml fresh 7H9 Complete. Each strain was then diluted in triplicate to a starting OD600 of ~0.033 in 1 ml 7H9 Complete. Culture were incubated at 33°C with vigorous shaking. OD600 readings were taken each day at ~24 hour intervals for ~72 hours, and the readings from each of three replicates was averaged for each timepoint per strain. Doubling times were calculated using GraphPad Prism 7. Briefly, a best-fit non-linear regression using an exponential growth model was applied to each data series, fixing y=0.033 for t=0.

RT-qPCR

RNA extractions were performed using the TRIzol Reagent (Thermo Fisher Scientific cat# 15596026) per manufacturer's instructions. cDNA was generated for each group to be tested using the iScript cDNA Synthesis Kit (BioRad cat# 1708890) with an input of 1 μg of RNA.

M. marinum *16S Burden Analysis*

M. marinum-specific 16S primers were designed based on 16S hypervariable regions identified as best able to distinguish between different *Mycobacteria spp*. (Chakravorty et al., 2007). F primer: 5'-CGATCTGCCCTGCACTTC-3'; R primer: 5'- CCACAGGACAT GAATCCCGT-3'. RT-qPCR was performed using the Power SYBR Green PCR Master Mix (Thermo Fisher Scientific cat# 4367659) per the manufacturer's instructions. β-actin transcript levels (zebrafish gene *actb1*) were used as the internal input control. F primer: 5'-CGAGCAGGAGATGGGAACC-3'; R primer: 5'-CAACGGAAACGCTCATTGC-3'.

Zebrafish tnfa Induction Analysis. Zebrafish *tnfa* cDNA was amplified using F primer:

5'-CAGGGCAATCAACAAGATGG-3'; R primer: 5'-TGGTCCTGGTCATCTCTCCA-3'. RT-qPCR was performed as described for *M. marinum* 16S cDNA. β-actin transcript levels were used as the internal input control.

Pazopanib Treatment

Pazopanib (Sigma-Aldrich cat# CDS023580) was used as described (Oehlers et al., 2015). Briefly, larvae were randomly assigned to two 100 mm petri dishes containing 40 ml of E3 media immediately following injection with TDM. To one dish, 40 μl of DMSO was added to achieve a final concentration of 0.1% v/v DMSO in E3 (vehicle group). To the other dish, 40 ul of a 250 μM stock of Pazopanib in DMSO was added to achieve a final concentration of 250 nM Pazopanib, 0.1% v/v DMSO in E3 (treatment group). Animals were kept under these conditions continually for the duration of the experiment.

QUANTIFICATION AND STATISTICAL ANALYSIS

Image Analysis

Image analysis was performed using ImageJ (NIH). Abnormal angiogenesis was measured by tracing the path of vasculature present between intersegmental vessels. Bacterial burden for each larva was measured by flattening image stacks in the relevant fluorescent channel using a maximum intensity projection, setting a threshold for signal above background, and measuring total fluorescent area. Background thresholds were held constant across all larva for a given time point and fluorescent channel.

TNF reporter induction in the transgenic line *TgBAC(tnf:GFP)* was measured for each larva by flattening image stacks in the relevant fluorescent channel using a maximum intensity projection, setting a threshold for signal above background, and measuring total fluorescent area. Background thresholds were held constant across all larva for a given time point and fluorescent channel.

The transgenic line *TgBAC(vegfaa:EGFP)* possesses a high baseline signal due to normal activation of *vegfaa* during development. Larvae were collected from a cross of adults heterozygous for the transgene in order to generate the largest possible pool of transgene-positive larvae possible from the pool of adults on hand, and as a result the background signal varied by as much as two-fold from larva to larva (i.e., one or two copies of the transgene). Because of this, *vegfaa* induction was measured in a slightly modified manner: image stacks were first flattened using a maximum intensity projection. Background for a given larva was then measured by recording the maximum value of fluorescent signal within an area of three uninfected somites. The resulting value was used to set the threshold for that larva, and area of signal above the threshold was measured for the infected region. This process was repeated for each individual larva.

Statistics

All statistics were performed using GraphPad Prism 7, and are noted for each analysis in the respective figure legends. Unless otherwise noted in the figure legends, all comparisons are as follows: comparison of the average of two groups only utilized Student's t-test; comparison of more than two groups utilized One-way ANOVA with Tukey's multiple comparison post-test. Comparison of any pair of contingency table datasets (absence vs. presence of phenotype) utilized Fisher's exact test. For clarity, contingency table data are displayed as percentage of total, with N=total number of animals listed above each bar. However, the statistical analyses were performed on the untransformed values. In all cases, minimum significance for rejecting the null hypothesis for a given comparison is $p<0.05$, denoted by *. ** denotes $p<0.01$; *** denotes $p<0.001$; and **** denotes $p< 0.0001$.